Coverage Probability and Achievable Rate Analysis of FFR-Aided Multi-User OFDM-Based MIMO and SIMO Systems

Suman Kumar, Sheetal Kalyani, Lajos Hanzo, *Fellow, IEEE*, and K. Giridhar, *Member, IEEE*

***Abstract*—Expressions are derived for the coverage probability and average rate of both multi-user multiple input multiple output (MU-MIMO) and single input multiple output (SIMO) systems in the context of a fractional frequency reuse (FFR) scheme. In particular, given a reuse region of $\frac{1}{3}$ (FR3) and a reuse region of 1 (FR1) as well as a signal-to-interference-plus-noise-ratio (SINR) threshold S_{th}, which decides the user assignment to either the FR1 or FR3 regions, we theoretically show that: 1) the optimal choice of S_{th} which maximizes the coverage probability is $S_{th} = T$, where T is the target SINR required for ensuring adequate coverage, and 2) the optimal choice of S_{th} which maximizes the average rate is given by $S_{th} = T'$, where T' is a function of the path loss exponent, the number of antennas and of the fading parameters. The impact of frequency domain correlation amongst the OFDM sub-bands allocated to the FR1 and FR3 cell-regions is analysed and it is shown that the presence of correlation reduces both the coverage probability and the average throughput of the FFR network. Furthermore, the performance of our FFR-aided MU-MIMO and SIMO systems is compared. Our analysis shows that the (2 × 2) MU-MIMO system achieves 22.5% higher rate than the (1 × 3) SIMO system and for lower target SINRs, the coverage probability of a (2 × 2) MU-MIMO system is comparable to a (1 × 3) SIMO system. Hence the former one may be preferred over the latter. Our simulation results closely match the analytical results.**

***Index Terms*—Author, please supply index terms/keywords for your paper. To download the IEEE Taxonomy go to http://www.ieee.org/documents/taxonomy_v101.pdf.**

AQ1

I. INTRODUCTION

ORTHOGONAL frequency division multiple access (OFDMA) based systems maintain orthogonality among the intra-cell users, but the radical OFDMA system deployments relying on a frequency reuse factor of unity suffer from inter-cell interference. As a remedy, inter-cell interference coordination (ICIC) schemes have been designed for minimizing the co-channel interference [1]. Fractional frequency reuse (FFR) [2] constitutes a low complexity ICIC scheme, which has been proposed for OFDMA based wireless networks such as IEEE WiMAX [3] and 3GPP LTE [4].

Manuscript received January 18, 2015; revised June 5, 2015; accepted August 1, 2015. The associate editor coordinating the review of this paper and approving it for publication was O. Oyman.

S. Kumar, S. Kalyani, and K. Giridhar are with the Indian Institute of Technology Madras, Chennai 600 036, India (e-mail: ee10d040@ee.iitm.ac.in; skalyani@ee.iitm.ac.in; giri@ee.iitm.ac.in).

AQ2

L. Hanzo is with the School of Electrical and Computer Science, University of Southampton, Southampton SO17 1BJ, U.K. (e-mail: lh@ecs.soton.ac.uk).

Color versions of one or more of the figures in this paper are available online at http://ieeexplore.ieee.org.

Digital Object Identifier 10.1109/TCOMM.2015.2465907

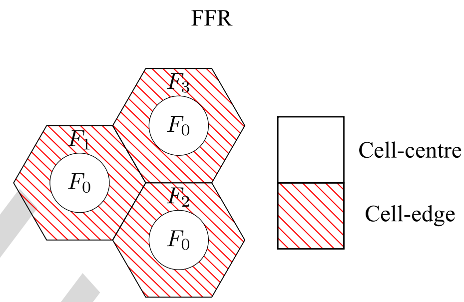

Fig. 1. Frequency allocation in FFR for three neighbouring cells with $\delta = 3$. The cell-centre users of all the cells rely on a common frequency band F_0, while the cell-edge users of the three cells occupy different frequency bands, namely F_1, F_2 and F_3.

Explicitly, FFR is a combination of frequency reuse 1 (FR1) and frequency reuse $\frac{1}{\delta}$ (FRδ). FR1 allocates all the frequencies to each cell, leading to a unity spatial reuse, hence results in a low-quality coverage due to the excessive inter-cell interference. On the other hand, FRδ allocates a fraction of $\frac{1}{\delta}$ of the frequencies to each cell and therefore reduces the area-spectral-efficiency, but improves the SINR. FFR strikes an attractive trade-off by exploiting the advantages of both FR1 and FRδ by relying on FR1 for the cell-centre users i.e. for those users who would experience less interference from the other cells, because they are close to their serving base station (BS). By contrast, FRδ is invoked for the cell-edge users i.e. for those users who would experience high interference afflicted by the co-channel signals emanating from the neighbouring cells in case of FR1, because they are far from their serving BS. Typically, there are two basic modes of FFR deployment: static and dynamic FFR [1]. In this paper, we consider the more practical static FFR scheme, where all the parameters are configured and kept fixed over a certain period of time [5]. Fig. 1 depicts a typical frequency allocation in the context of the FFR scheme for three adjacent cells, where F_1, F_2 and F_3 each use x% of the total spectrum, hence F_0 uses $(100 - 3x)$% of the spectrum.

FFR schemes have been lavishly studied using both system level simulations and theoretical analysis [6]–[11]. The optimization of FFR relying on a distance threshold[1] or SINR threshold[2]

[1]Based on a pre-determined distance from the BS, the subscribers are divided into cell-centre as well as cell-edge users and hence here the design parameter is a distance threshold (R_{th}).

[2]Based on a pre-determined SINR, the subscribers are divided into cell-centre as well as cell-edge users and here the design parameter is the SINR threshold (S_{th}).

0090-6778 © 2015 IEEE. Personal use is permitted, but republication/redistribution requires IEEE permission.
See http://www.ieee.org/publications_standards/publications/rights/index.html for more information.

IEEE Proof

has been studied using graph theory in [6] and convex optimization in [7]. Specifically, it has been shown in [7] that the optimal frequency reuse factor is FR3 for the cell-edge users. The average cell throughput of an FFR system was derived in [8] as a function of the distance threshold. It was shown in [9] that there exists an optimal radius threshold for which the average rate becomes maximum. The performance of FFR and soft frequency reuse (SFR) has been studied in [12] under both fully loaded and partially loaded scenarios. An algorithm was proposed in [13] for enhancing the network capacity and the cell-edge performance for a dynamic SFR deployment relying on realistic irregularly shaped cells. A fuzzy logic based generic model was proposed for deriving different frequency reuse schemes in [14]. As a further development, an FFR based 3-cell network-MIMO based tri-sector BS architecture was presented in [15]. FFR and SFR are compared in the presence of correlated interferers in [16]. The optimal configuration of FFR is determined in [17] for a high-density wireless cellular network. The authors of [18] have proposed a distributed and adaptive solution for interference coordination based on the center of gravity of users in each sector. An optimal FFR and power control scheme which can coordinate the interference among the heterogeneous nodes is proposed in [19].

An analytical framework of calculating both the coverage probability (CP_r) and the average rate of FFR schemes was presented in [10] and [11] for homogeneous single input single output (SISO) and MIMO heterogeneous networks, respectively, using a Poisson point process (PPP). However, the authors of [10], [11] assumed having an unplanned FFR network, where the cells using the same frequency set are randomly allocated. Hence, two cells using the same frequency for the cell-edge users may in fact be co-located [10], [11]. However, in case of FFR based deployments the regions using the same frequency are typically planned to be as far apart as possible and our focus is on these types of deployments. An FFR-aided distributed antenna system (DAS) and an FFR-aided picocell was studied in [20] and [21]. While, an FFR-aided femtocell has been extensively studied in [22]–[26].

However, most of the work based on FFR has considered the conventional SISO case. To the best of our knowledge, no prior work has analytically derived the optimal SINR threshold for FFR, when the number of antennas is high at the transmitter and/or at the receiver. Hence, in this work, we derive both the CP_r and the average achievable rate expressions of FFR in the presence of both MU-MIMO as well as of SIMO systems and derive the optimal SINR threshold corresponding to the desired CP_r and throughput. Furthermore, the performance of FFR-aided MU-MIMOs is compared to that of FFR in the presence of a SIMO system.

The key benefit of MU-MIMO is their ability to improve the spectral efficiency, which has been extensively studied in a single-cell context in the presence of AWGN [27]–[29]. However, it has been shown in [30], [31] with the help of simulation, that the efficiency of MU-MIMOs is significantly eroded in a multi-cell environment due to interference, especially in the cell-edge region. FFR is capable of significantly improving the cell-edge coverage since it uses FR3 for the cell-edge users. Hence we study FFR-aided MU-MIMOs and quantify their average throughput as well as coverage probability.

Furthermore, we carefully examine the correlation of the sub-bands F_0, F_1, F_2 and F_3 in Fig. 1 used in the FFR system considered. All prior work on FFR has assumed that the sub-bands experience independent fading, which is mathematically convenient, but practically not realisable. Indeed, when we consider practical transmission block based modulation such as OFDM, the channel's delay spread is assumed to be confined to the cyclic prefix of the OFDM symbol. Such a limited-duration (typically less than 20% of the useful OFDM symbol duration) impulse response will result in correlation amongst the adjacent frequency domain OFDM sub-channels. More explicitly, unless the sub-bands $F_0 \cdots F_3$ are spaced apart by more than the reciprocal of the delay spread, correlation will exist. Since the delay spread experienced in the downlink is user-dependent, it is virtually impossible to ensure that the sub-bands F_i in Fig. 1 are independent for each user scheduled in the downlink. Therefore, in our analysis we will specifically take into account the correlation of the sub-bands. For FFR-aided MU-MIMO and SIMO systems, the expressions of CP_r and average rate are derived and the following new results are presented:

(a) The optimal SINR threshold that maximizes the CP_r of FFR is derived for a given T. We show that the optimal S_{th} (denoted by $S_{opt,C}$) is $S_{th} = T$ for both the MU-MIMO and SIMO system, and if we choose the SINR threshold to be $S_{opt,C}$, then the achievable CP_r of FFR is higher than that of FR3. The improvement of the FFR CP_r over that of FR3 is due to the resultant sub-band diversity gain achieved by the systems when a user is classified as either a cell-centre or a cell-edge user.

(b) The optimal SINR threshold that maximizes the average rate of FFR is derived. We show that the optimal S_{th} (denoted by $S_{opt,R}$) is equal to T' for both MU-MIMO and SIMO systems, where T' is a fixed SINR value, which depends on the system parameters such as the path loss exponent, the number of antennas, the fading parameters, etc.

(c) The correlation of the sub-bands always degrades both the CP_r and the average rate of the FFR-aided MU-MIMO and SIMO systems.

(d) The performance of FFR-aided MU-MIMO and SIMO systems is compared. It is shown that system designer may choose the (2×2) MU-MIMO system over (1×3) SIMO system of FFR scheme as MU-MIMO achieves significant gain in average rate over SIMO.

We will demonstrate that our analytical results are in close agreement with the simulation results. Moreover, it is shown that at optimal S_{th}, the FFR achieves significantly high gain in CP_r than that of average rate with respect to FR1 and hence this scheme would be more useful when coverage gain is essentially required. Therefore, FFR-aided MU-MIMO provides both high average rate and satisfactory CP_r for a lower value of N_a.

II. System Model

A homogeneous macrocell network relying on hexagonal tessellation and on an inter cell site distance of $2R$ is considered,

IEEE Proof

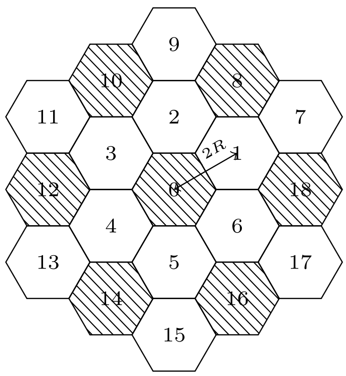

Fig. 2. Hexagonal structure of 2-tier macrocell. Interference for 0th cell in FR1 system is contributed form all the neighbouring 18 cells, while in a FR3 system it is contributed only from the shaded cells.

as shown in Fig. 2. Both a MU-MIMO and a SIMO system is considered. We assume that in the MU-MIMO case each user is equipped with N_r receive antennas, while the BS is equipped with N_t transmit antennas and that $N_t = N_r$. Our focus is on the downlink and hence N_t transmit antennas are used for transmission, while the N_r receive antennas at the UE are used for reception. We also assume that all N_t transmit antennas at the BS are utilized to transmit N_t independent data steams to its own N_t users. A linear minimum mean-square-error (LMMSE) receiver [32] is considered. In order to calculate the post-processing SINR of this LMMSE receiver, it is assumed that the $(N_r - 1)$ closest interferers can be completely cancelled using the antennas at the receiver.[3] For example, in the MU-MIMO case, the user will not experience any intra-tier interference emanating from the serving BS as $N_t = N_r$. In the SIMO case each user is equipped with N_r antennas. The SINR $\eta_t(r)$ of a user in the MU-MIMO system and the SINR $\eta_r(r)$ of a user in the SIMO system located at r meters from its serving BS are given by

$$\eta_t(r) = \frac{gr^{-\alpha}}{\frac{\sigma^2}{P} + I_t}, \quad I_t = \sum_{i \in \psi} \sum_{j=1}^{N_t} h_{ij} d_i^{-\alpha} \tag{1}$$

and

$$\eta_r(r) = \frac{gr^{-\alpha}}{\frac{\sigma^2}{P} + I_r}, \quad I_r = \sum_{i \in \psi_r} h_{ij} d_i^{-\alpha}, \tag{2}$$

respectively, where the transmit power of a BS is denoted by P. Here ψ is the set of interfering BSs in the FR1 network and ψ_r denotes all the interfering BSs, excluding the nearest $(N_r - 1)$ interferers, while N_t denotes the number of transmit antennas. The standard path loss model of $\|x\|^{-\alpha}$ is assumed, where $\alpha \geq 2$ is the path loss exponent and $\|x\|$ is the distance of a user from the BS. We assumed that the users are at least at a distance of d away from the BS.[4] The noise power is denoted by σ^2. Here, r and d_i are the distances from the user to the serving BS and to the i^{th} interfering BS, respectively, while g and h_i denote the corresponding channel fading power, which are independent and identically exponentially distributed (i.i.d.) with a unit mean, i.e., $g \sim \exp(1)$ and $h_i \sim \exp(1) \forall\, i$. In MU-MIMO case, h_{ij} is the channel's fading power from the j^{th} antenna of the i^{th} interfering BS to the user and it is i.i.d. with a unit mean. Without loss of generality we have considered a user in the 0^{th} cell of Fig. 2 in our analysis.

Similar to [10], the subscribers are classified as cell-centre users and cell-edge users based on the SINR at the mobile station. If the calculated SINR of a user is lower than the specified SINR threshold S_{th}, the user is classified as a cell-edge user. Otherwise, the user is classified as a cell-centre user. Typically, FFR divides the whole frequency band into a total of $(1 + \delta)$ parts, where F_0 is allocated to all the cells for the cell-centre users, as seen in Fig. 1. One of the $\{1, \cdots, \delta\}$ parts is assigned to the cell-edge users in each cell in a planned fashion. The users are assumed to be uniformly distributed in a cell and all resource blocks are uniformly shared among the users. The transmit power is assumed to be fixed. If we have $\eta_t(r)$(or $\eta_r(r)) \geq S_{th}$ for a user, then the user will continue to experience the same fading power, i.e., g and h_i from the user to the serving BS and to the i^{th} interfering BS, respectively. However, if we have $\eta_t(r)$(or $\eta_r(r)) < S_{th}$ for a user, the user is allocated another sub-band (from the set of sub-bands assigned to cell-edge users) and it experiences a new fading power, i.e., $\hat{g}$ and $\hat{h}_i$ from the user to the serving BS and to the i^{th} interfering BS, respectively. Based on the coherence bandwidth of the OFDM system, and the bands associated with F_0 to F_3 in Fig. 1 is is possible that $\hat{g}$ and $\hat{h}_i$ are either correlated with or independent of g and h_i, respectively. Note that g, $\hat{g}$, h_i, and $\hat{h}_i$ are the channel gains in the frequency domain and the term correlation is used for referring to frequency domain correlation in this paper. The correlation depends both on the particular user's channel conditions and on the instantaneous coherence bandwidth with respect to the FFR frequency bands. To better understand the impact of correlation among the sub-bands on the FFR system's performance, in this paper, we consider the following two extreme cases:

Case 1: g and $\hat{g}$ are independent and also h_i as well as $\hat{h}_i$, are independent for all i.

Case 2: g and $\hat{g}$ are fully correlated and also h_i as well as $\hat{h}_i$, are fully correlated for all i.

In reality these channel output powers may be partially correlated, but the analysis of partial (arbitrary) correlation is quite complicated and hence it is beyond the scope of this work. However, the analysis of the above two extreme cases we believe, is sufficient for understanding the impact of correlation among the sub-bands.

III. Coverage Probability Analysis of FFR

In this section, we first derive the CP_r of both the MU-MIMO and SIMO system considered, which is defined as the probability that a randomly chosen user's instantaneous SINR $\eta_t(r)$ is higher than T. This defines, the average fraction of users are having an SINR higher than the target SINR. The coverage probability is determined by the complementry cumulative distribution function of the SINR over the network. The

[3]It is widely exploited that using the LMMSE receiver $(N_r - 1)$ interferers can be mitigated, where N_r is the number of receive antennas [32]. However, for simplicity, we assume that the $N_r - 1$ closest interferers can be completely cancelled.

[4]Typically, the path loss model is assumed to be $\max\{d, \|x\|\}^{-\alpha}$.

IEEE Proof

CP_r of a user who is at a distance of r meters from the BS in a FR1-aided MU-MIMO scenario is given by

$$P_1(T,r) = P[\eta_t(r) > T] = P\left[g > Tr^{\alpha} I_t + Tr^{\alpha}\frac{\sigma^2}{P}\right], \quad (3)$$

where I_t is defined in (2). Since $g \sim \exp(1)$, $h_{ij} \sim \exp(1)$, and h_{ij} are i.i.d., $P_1(T,r)$ is given by

$$P_1(T,r) = E_{h_{ij}}\left[e^{-Tr^{\alpha} I_t - Tr^{\alpha}\frac{\sigma^2}{P}}\right] = \prod_{i\in\psi}\prod_{j=1}^{N_t} E_{h_{ij}}\left[e^{-Tr^{\alpha} h_{ij} d_i^{-\alpha}}\right] \times e^{-Tr^{\alpha}\frac{\sigma^2}{P}} = \prod_{i\in\psi}\left(\frac{1}{1+Tr^{\alpha}d_i^{-\alpha}}\right)^{N_t} e^{-Tr^{\alpha}\frac{\sigma^2}{P}}, \quad (4)$$

where ψ is the set of interfering BSs in a FR1 network. Similarly, the CP_r of a user located at a distance of r meters from the BS in a FR3 network can be formulated as

$$P_3(T,r) = \prod_{i\in\phi}\left(\frac{1}{1+Tr^{\alpha}d_i^{-\alpha}}\right)^{N_t} e^{-Tr^{\alpha}\frac{\sigma^2}{P}} \quad (5)$$

where ϕ is the set of interfering cells in the FR3 scheme, which is a function of the frequency reuse plan. Also, the CP_r of a user in the SIMO-based FR1 network and in a FR3 network can be expressed as

$$P_1(T,r) = \prod_{i\in\psi_r}\frac{1}{1+Tr^{\alpha}d_i^{-\alpha}} e^{-Tr^{\alpha}\frac{\sigma^2}{P}} \quad \text{and}$$
$$P_3(T,r) = \prod_{i\in\phi_r}\frac{1}{1+Tr^{\alpha}d_i^{-\alpha}} e^{-Tr^{\alpha}\frac{\sigma^2}{P}}. \quad (6)$$

Here ϕ_r denotes the set of interfering cells in the FR3 scheme excluding the nearest $(N_r - 1)$ interferers. Let us now derive the CP_r of FFR for both the independent and correlated cases.

A. *Case 1: g and $\hat{g}$ are Independent as Well as h_i and $\hat{h}_i$ are Also Independent for all i*

The CP_r $P_{F,c}(r)$ of a cell-centre user who is at a distance of r meters from the 0^{th} BS in a FFR-aided MU-MIMO scenario is given by

$$P_{F,c}(r) \overset{(a)}{=} P[\eta_t(r) > T | \eta_t(r) > S_{th}] = P\left[\frac{gr^{-\alpha}}{I_t+\frac{\sigma^2}{P}} > T \middle| \frac{gr^{-\alpha}}{I_t+\frac{\sigma^2}{P}} > S_{th}\right],$$

where (a) follows from the fact that a cell-centre user has SINR $\geq S_{th}$. Upon applying Bayes' rule, one can rewrite $P_{F,c}(r)$ as

$$P_{F,c}(r) = \frac{P\left[\frac{gr^{-\alpha}}{I_t+\frac{\sigma^2}{P}} > T, \frac{gr^{-\alpha}}{I_t+\frac{\sigma^2}{P}} > S_{th}\right]}{P\left[\frac{gr^{-\alpha}}{I_t+\frac{\sigma^2}{P}} > S_{th}\right]} = \frac{\prod_{i\in\psi}\left(\frac{1}{1+\max\{T,S_{th}\}r^{\alpha}d_i^{-\alpha}}\right)^{N_t} e^{-\max\{T,S_{th}\}r^{\alpha}\frac{\sigma^2}{P}}}{\prod_{j\in\psi}\left(\frac{1}{1+S_{th}r^{\alpha}d_j^{-\alpha}}\right)^{N_t} e^{-S_{th}r^{\alpha}\frac{\sigma^2}{P}}}. \quad (7)$$

Similarly, the CP_r of a cell-edge user who is at a distance of r meters from the BS in the FFR-aided MU-MIMO case $P_{F,e}(r)$ is given by

$$P_{F,e}(r) = P\left[\hat{\eta}_t(r) > T | \eta_t(r) < S_{th}\right] = \frac{P\left[\frac{\hat{g}r^{-\alpha}}{\hat{I}_t+\frac{\sigma^2}{P}} > T, \frac{gr^{-\alpha}}{I_t+\frac{\sigma^2}{P}} < S_{th}\right]}{P\left[\frac{gr^{-\alpha}}{I_t+\frac{\sigma^2}{P}} < S_{th}\right]}.$$

Here, the cell-edge user will experience the new interference term of $\hat{I}_t = \sum_{i\in\phi}\sum_{j=1}^{N_t}\hat{h}_{ij}d_i^{-\alpha}$ and the new channel power $\hat{g}$, i.e. a new SINR $\hat{\eta}(r)$ due to the fact that the cell-edge user is now a FR3 user. Basically, $\hat{\eta}(r)$ denotes the SINR experienced by the user at a distance of r meters from the BS in a FR3 system and is given by

$$\hat{\eta}(r) = \frac{\hat{g}r^{-\alpha}}{\hat{I}_t+\frac{\sigma^2}{P}}, \quad \hat{I}_t = \sum_{i\in\phi}\sum_{j=1}^{N_t}\hat{h}_{ij}d_i^{-\alpha}. \quad (8)$$

Since both g and $\hat{g}$ as well as h_i and $\hat{h}_i$ are assumed to be i.i.d, $P_{F,e}(r)$ can be simplified to

$$P_{F,e}(r) = P\left[\frac{\hat{g}r^{-\alpha}}{\hat{I}_t+\frac{\sigma^2}{P}} > T\right] = P_3(T,r). \quad (9)$$

Let us now derive the CP_r $P_f(r)$ of a user in the FFR-aided MU-MIMO system, which can be written as

$$P_F(r) = P_{F,c}(r)P[\eta_t(r) > S_{th}] + P_{F,e}(r)P[\eta_t(r) < S_{th}]. \quad (10)$$

Here, the first term denotes the CP_r contributed by the cell-centre users, while the second term denotes the contribution of the cell-edge users. By using the expression in (7) for $P_{F,c}(r)$ and the expression in (9) for $P_{F,e}(r)$, (10) can be simplified to

$$P_F(r) = \prod_{i\in\psi}\left(\frac{1}{1+\max\{T,S_{th}\}r^{\alpha}d_i^{-\alpha}}\right)^{N_t} e^{-\max\{T,S_{th}\}r^{\alpha}\frac{\sigma^2}{P}} + P_3(T,r) - P_3(T,r)P_1(S_{th},r). \quad (11)$$

Lemma 1: The optimum S_{th} (denoted by $S_{opt,C}$) that maximizes the FFR-aided coverage probability is $S_{th} = T$, and when the SINR threshold is set to $S_{opt,c}$, the coverage probability of FFR becomes higher than that of FR3.

Proof: See Appendix A for the proof. □

B. *Case 2: g and $\hat{g}$ are Completely Correlated as Well as h_i and $\hat{h}_i$ are Also Completely Correlated for all i*

Note that the centre CP_r is the same for both the above Case 1 and for this case, since a user does not change its sub-band, when it becomes a cell-centre user because if $\eta_t(r) \geq S_{th}$ for a user, then it will continue to experience the same fading power. However, the edge CP_r is different in Case 1 as well as Case 2, and in this scenario the CP_r $P_{F,e}(r)$ of a cell-edge user,

IEEE Proof

who is at a distance of r meters from the BS in our FFR network is given by

$$P_{F,e}(r)=P\left[\hat{\eta}_t(r)>T|\eta_t(r)<S_{th}\right]=\frac{P\left[\hat{\eta}_t(r)>T,\,\eta_t(r)<S_{th}\right]}{P\left[\eta_t(r)<S_{th}\right]}. \quad (12)$$

Substituting the value of $P_{F,c}$ and $P_{F,e}$ from (7) and (12) into Eq. (10), the CP$_r$ $P_f(r)$ in our FFR network can be written as

$$P_F(r)=\prod_{i\in\psi}\left(\frac{1}{1+\max\{T,S_{th}\}r^{\alpha}d_i^{-\alpha}}\right)^{N_t}e^{-\max\{T,S_{th}\}r^{\alpha}\frac{\sigma^2}{P}} + P\left[\hat{\eta}_t(r)>T,\,\eta_t(r)<S_{th}\right]. \quad (13)$$

Recall that $\eta_t(r)$ and $\hat{\eta}_t(r)$ represent the SINR experienced by a user in an FR1 and an FR3 system, respectively. Note that even though g and $\hat{g}$ as well as h_i and $\hat{h}_i$ are completely correlated, $\eta_t(r)$ is not the same as $\hat{\eta}_t(r)$, because the set of interferers are different in the denominator of the $\eta_t(r)$ and $\hat{\eta}_t(r)$ expressions given in (2) and (8), respectively, i.e., ψ corresponds to the set of interferers in the FR1 network, while ϕ corresponds to the set of interferers in the FR3 network. Since g and $\hat{g}$ are completely correlated and h_i and $\hat{h}_i$ are also completely correlated for all i, we use the following transformation to further simplify $P_F(r)$:

$$P\left[\hat{\eta}_t(r)>T,\,\eta_t(r)<S_{th}\right]=P\left[\hat{\eta}_t(r)>T,\,\hat{\eta}_t(r)<\hat{S}_{th}\right]. \quad (14)$$

Basically instead of marking a user as a cell-edge user based on the FR1 SINR $\eta_t(r)$, we mark them on the basis of the FR3 SINR $\hat{\eta}_t(r)$ by introducing a new SINR threshold $\hat{S}_{th}$. In other words, we introduce a new SINR threshold $\hat{S}_{th}$ for ensuring that if for any user we have $\eta_t(r)<S_{th}$, then for the same user we have $\hat{\eta}_t(r)<\hat{S}_{th}$ and vice-versa. The threshold $\hat{S}_{th}$ is computed using the relationship of $P[\eta_t(r)<S_{th}]=P[\hat{\eta}_t(r)<\hat{S}_{th}]$. This ensures that the same user is marked as a cell-edge user for both reuse patterns FR1 and FR3. Now, using the transformation given in (14), $P_F(r)$ can be simplified to

$$P_F(r)=\prod_{i\in\psi}\left(\frac{1}{1+\max\{T,S_{th}\}r^{\alpha}d_i^{-\alpha}}\right)^{N_t}e^{-\max\{T,S_{th}\}r^{\alpha}\frac{\sigma^2}{P}} + P\left[\hat{\eta}(r)>T\right]-P\left[\hat{\eta}(r)>\max\{\hat{S}_{th},T\}\right]. \quad (15)$$

In this case, to obtain the optimum $S_{opt,C}$, we consider the following two possibilities: (*i*) $S_{th}\geq T$, (*ii*) $S_{th}<T$.

(i) $S_{th}\geq T$: In this scenario, $CP_f(r)$ can be expressed in terms of T as:

$$P_F(r,S_{th}\geq T)=\prod_{i\in\psi}\frac{1}{1+S_{th}r^{\alpha}d_i^{-\alpha}}e^{-S_{th}r^{\alpha}\frac{\sigma^2}{P}} + P_3(T,r)-P_3(\hat{S}_{th},r). \quad (16)$$

Since we have $P_3(\hat{S}_{th},r)=P_1(S_{th},r)$ and $P_1(S_{th},r)=\prod_{i\in\psi}\left(\frac{1}{1+S_{th}r^{\alpha}d_i^{-\alpha}}\right)^{N_t}e^{-S_{th}r^{\alpha}\frac{\sigma^2}{P}}$, hence

$$P_F(r,S_{th}\geq T)=P_3(T,r). \quad (17)$$

(ii) $S_{th}<T$: In this case $P_f(r)$ can be formulated in terms of T as:

$$P_F(r,S_{th}<T)=\prod_{i\in\psi}\left(\frac{1}{1+Tr^{\alpha}d_i^{-\alpha}}\right)^{N_t}e^{-Tr^{\alpha}\frac{\sigma^2}{P}} + P_3(T,r)-P_3\left(\max\{\hat{S}_{th},T\},r\right). \quad (18)$$

Note that when $S_{th}<T$, $\hat{S}_{th}$ may be higher or lower than T. When $\hat{S}_{th}>T$,

$$P_3\left(\max\{\hat{S}_{th},T\},r\right)=P_3(\hat{S}_{th},r)=P_1(S_{th},r)>P_1(T,r) \quad (19)$$

since $S_{th}<T$. And when $\hat{S}_{th}<T$, we have:

$$P_3\left(\max\{\hat{S}_{th},T\},r\right)=P_3(T,r)>P_1(T,r). \quad (20)$$

Hence, we arrive at:

$$P_F(r,S_{th}<T)=\prod_{i\in\psi}\left(\frac{1}{1+Tr^{\alpha}d_i^{-\alpha}}\right)^{N_t}e^{-Tr^{\alpha}\frac{\sigma^2}{P}} + P_3(T,r)-P_3\left(\max\{\hat{S}_{th},T\},r\right)<P_3(T,r). \quad (21)$$

Comparing the FFR CP$_r$ for $S_{th}\geq T$ and $S_{th}<T$ given by (17) and (21), respectively, it becomes apparent that $P_F(r,S_{th}\geq T)>P_F(r,S_{th}<T)$. In other words, when the fading is fully correlated across the sub-bands, the optimal choice of the SINR threshold is $S_{th}\geq T$ and at the optimal SINR threshold the FFR scheme succeeds in achieving the FR3 CP$_r$. Unlike for Case 1, the FFR CP$_r$ is not better than the FR3 CP$_r$ since there is no sub-band diversity gain, when a user moves from the cell-centre to the cell-edge region.

In order to find the CP$_r$ for a typical user, we have to calculate the probability density function (pdf) of r, which is the distance between the 0^{th} BS (serving BS) and the desired user. To calculate this pdf, we model the cell shape by an inner circle within a hexagonal cell [33], and assume that the users are uniformly distributed. Therefore, the pdf $f_R(r)$ of r is given by

$$f_R(r)=\begin{cases}\frac{2r}{R^2},\ r\leqslant R\\ 0,\ r>R.\end{cases} \quad (22)$$

IV. Average Rate

In this section, we derive the average rate of both the FFR-aided MU-MIMO as well as of its SIMO counterpart and find the optimum value of S_{th} (denoted by $S_{opt,R}$) for which the average rate is maximum. The average rate of the system is given by $R=E[\ln(1+\text{SINR})]$. In order to derive the average rate[5] for the FFR system, we have to consider its sub-band allocation. Since the users are uniformly distributed, the specific sub-band allocated to the cell-centre users and cell-edge users are given by [9], [10] $N_c=N_tP_{F,c}$ and $N_e=\frac{N_t-N_c}{3}$, where $P_{F,c}$ denotes the specific fraction of cell-centre users, while N_t, N_c and N_e denote the total band, cell-centre sub-band and cell-edge

[5]An interference limited system is assumed for simplicity, which implies ignoring the effects of noise. However, the derivation of the average rate can be readily extended to the case, where the thermal noise is also considered.

IEEE Proof

sub-band, respectively. Let us now derive the average rate for the planned FFR-aided MU-MIMO case.

A. Average Rate in the FR1 and FR3 Systems

The average rate of a user at a distance r is $E[\ln(1+\eta_t(r))]$. By exploiting the fact that for a positive random variable $X = \ln(1+\eta_t(r))$ we have $E[X] = \int_{t>0} P(X>t)\mathrm{d}t$, the rate $R_1(r)$ can be rewritten as

$$R_1(r) = \int_{t>0} P[\ln(1+\eta_t(r)) > t]\mathrm{d}t = \int_{t>0} P[\eta_t(r) > e^t - 1]\mathrm{d}t$$
$$= \int_{t>0} \prod_{j\in\psi} \left(\frac{1}{1+(e^t-1)r^\alpha d_j^{-\alpha}}\right)^{N_t} \mathrm{d}t, \quad (23)$$

which follows from (3) and (4). Let us now determine the average rate of the FR1 system, where spatially averaged rate R_1 can be expressed as

$$R_1 = \int_0^R \int_{t>0} \prod_{j\in\psi} \left(\frac{1}{1+(e^t-1)r^\alpha d_j^{-\alpha}}\right)^{N_t} \mathrm{d}t f_R(r)\mathrm{d}r. \quad (24)$$

The average rate of FR3 can be obtained in a similar fashion, which is given by

$$R_3 = \int_0^R \int_{t>0} \prod_{i\in\phi} \left(\frac{1}{1+(e^t-1)r^\alpha d_i^{-\alpha}}\right)^{N_t} \mathrm{d}t f_R(r)\mathrm{d}r. \quad (25)$$

B. Average Rate of the FFR System, When the Sub-Bands are Independent

Lemma 2: The average rate of the FFR-aided MU-MIMO system is given by

$$R_f = \int_0^R \int_{t>0} \left(\prod_{j\in\psi} \left(\frac{1}{1+\max\{e^t-1, S_{th}\} r^\alpha d_j^{-\alpha}}\right)^{N_t} + \frac{1}{3}\prod_{i\in\phi} \frac{P[\eta_t(r) < S_{th}]}{\left(1+(e^t-1)r^\alpha d_i^{-\alpha}\right)^{N_t}} \right) \mathrm{d}t f_R(r)\mathrm{d}r. \quad (26)$$

Proof: See Appendix B for the proof. □

Similarly, the average rate of the FFR-aided SIMO system is given by

$$R_f = \int_0^R \int_{t>0} \left(\prod_{j\in\psi_r} \frac{1}{1+\max\{e^t-1, S_{th}\} r^\alpha d_j^{-\alpha}} + \frac{1}{3}\prod_{i\in\phi_r} \frac{P[\eta_r(r) < S_{th}]}{1+(e^t-1)r^\alpha d_i^{-\alpha}} \right) \mathrm{d}t f_R(r)\mathrm{d}r. \quad (27)$$

C. Optimum Value of the SIR Threshold $S_{opt,R}$, When the Sub-Bands are Independent

The optimum value of S_{th} (denoted by $S_{opt,R}$) for which the average rate of the FFR system is maximized is derived and it is shown to be a function of both the number of antennas and of the path loss exponent.

Lemma 3: The value of S_{th} which maximizes the average rate of the FFR system is $S_{opt,R} = T'$, where T' can be obtained as the solution of equation given in (28), shown at the bottom of the page, where, $K(r)$ is defined later in (47).

Proof: See Appendix C for the proof. □

Note that the optimal S_{th} of the SIMO scenario can be derived by following the method of the MU-MIMO case and it is $S_{opt,R} = T'$, where T' can be obtained as the solution of the equation given in (29), shown at the bottom of the page, where we have $K(r) = \frac{1}{3}\int_{t>0} \prod_{i\in\phi_r} \frac{1}{1+(e^t-1)r^\alpha d_i^{-\alpha}} \mathrm{d}t$.

Fig. 3 plots the optimal SINR threshold S_{th} versus the number of antennas for different path loss exponent. It can be observed for the MU-MIMO case that as the number of transmit antennas is reduced, $S_{opt,R}$ increases. Intuitively, as the number of transmit antennas decreases, the interference experienced by the user would decrease as the interference from the other cell decrease. Thus, the average SINR of all users increases. Hence, the optimal SINR threshold increases in order to balance the ratio of cell-edge users and cell-centre users. Similarly, as the number of receive antennas increases, the average SINR increases in SIMO scenario, because more antennas are capable of cancelling more of the closest interferers. Hence, $S_{opt,R}$ increases

$$\int_0^R \left(\frac{\left(K(r) - \ln(1+T')\right) \sum_{i\in\psi} \left(1+T' r^\alpha d_i^{-\alpha}\right)^{N_t-1} r^\alpha d_i^{-\alpha} \left(\prod_{j\in\psi\setminus i} \left(1+T' r^\alpha d_j^{-\alpha}\right)^{N_t} \right)}{\left(\prod_{j\in\psi} \left(1+T' r^\alpha d_j^{-\alpha}\right)\right)^{2N_t}} \right) f_R(r)\mathrm{d}r = 0, \quad (28)$$

$$\int_0^R \left(\frac{\left(K(r) - \ln(1+T')\right) \sum_{i\in\psi_r} r^\alpha d_i^{-\alpha} \left(\prod_{j\in\psi_r\setminus i} \left(1+T' r^\alpha d_j^{-\alpha}\right) \right)}{\left(\prod_{j\in\psi_r} \left(1+T' r^\alpha d_j^{-\alpha}\right)\right)^{2}} \right) f_R(r)\mathrm{d}r = 0, \quad (29)$$

IEEE Proof

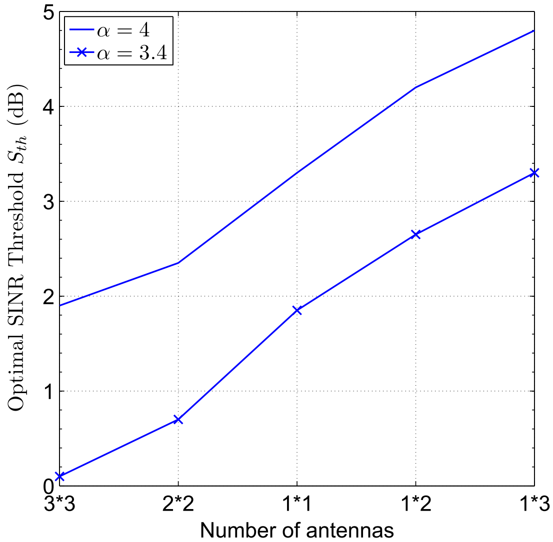

Fig. 3. Optimal SINR threshold S_{th} evaluated using (28) and (29) versus the number of antennas for different path-loss exponents.

in order to balance the ratio of cell-centre users and cell-edge users. Furthermore, as the path loss exponent decreases, the average SIR of all the users decreases and hence $S_{opt,R}$ decreases.

D. *Average Rate of the FFR System, When the Sub-Bands are Completely Correlated*

In this subsection first we derive the average rate $R_f(r)$ of the FFR system for the MU-MIMO case. The average rate of the FFR system given in (39) can be rewritten as

$$R_f(r) = R_c(r)P\left[\eta_t(r) > S_{th}\right] + \frac{1}{3}R_e(r)P\left[\eta_t(r) < S_{th}\right]. \quad (30)$$

Note that the first term $R_c(r)P[\eta_t(r) > S_{th}]$ denotes the average rate contributed by the cell-centre users and it is the same regardless, whether the fading of the bands is correlated or independent across the sub-bands. Similar to the average rate of the FFR system given in (39), the factor $\frac{1}{3}$ is introduced in the second term, since a frequency reuse factor of $\frac{1}{3}$ is invoked for the cell-edge users. In other words, only one third of the cell-edge frequency $(F_1 + F_2 + F_3)$ is used for the cell-edge users and hence the factor $\frac{1}{3}$ multiplies the second term of (30). Now, using the expression of $R_e(r)$ in (42), $R_e(r)P[\eta_t(r) < S_{th}]$ can be written as

$$R_e(r)P\left[\eta_t(r) < S_{th}\right] = \int_{t>0} P\left[\hat{\eta}_t(r) > e^t - 1,\, \eta_t(r) < S_{th}\right] \mathrm{d}t. \quad (31)$$

Using the transformation in (14), $R_e(r)P[\eta_t(r) < S_{th}]$ can be simplified to

$$R_e(r)P\left[\eta_t(r) < S_{th}\right] = \int_{t>0} P\left[\hat{\eta}_t(r) > e^t - 1\right] - P\left[\hat{\eta}_t(r) > \max\{e^t - 1, \hat{S}_{th}\}\right] \mathrm{d}t. \quad (32)$$

Using the result of (25), $R_e(r)P[\eta(r) < S_{th}]$ can be further simplified to

$$R_e(r)P\left[\eta_t(r) < S_{th}\right] = \int_{t>0} \prod_{i\in\phi} \frac{1}{1 + (e^t - 1)r^\alpha d_i^{-\alpha}} - \prod_{i\in\phi} \frac{1}{1 + \max\{e^t - 1, \hat{S}_{th}\} r^\alpha d_i^{-\alpha}} \mathrm{d}t. \quad (33)$$

Finally, substituting back (41) as well as (33) into (30) and then averaging over the spatial dimension, the average rate of the FFR system is given as

$$R_f = \int_0^R \int_{t>0} \prod_{j\in\psi} \frac{1}{1+\max\{e^t-1, S_{th}\} r^\alpha d_j^{-\alpha}} + \frac{1}{3}\left(\prod_{i\in\phi} \frac{1}{1+(e^t-1) r^\alpha d_i^{-\alpha}} - \prod_{i\in\phi} \frac{1}{1+\max\{e^t-1, \hat{S}_{th}\} r^\alpha d_i^{-\alpha}} \right) \mathrm{d}t f_R(r) \mathrm{d}r. \quad (34)$$

V. Simulation Results

In this section, we provide the simulation results in order to verify our analytical results In the simulations, we have considered the classic 19 cell system associated with a hexagonal structure having a radius of 1000 meters. A LTE system having a 10 MHz bandwidth, 50 physical resource blocks (PRB) and 25 users is considered for each cell. The users are assumed to be uniformly distributed in a cell and similarly, all resource blocks are uniformly shared among users. In other words, if there are K users and R resource blocks then each user is assigned $\frac{R}{K}$ resource blocks. For each user we generate the channel fading power corresponding to its own channel as well as that corresponding to the 18 interferers and then compute the SIR per user per PRB. If a user having an SIR higher than S_{th} over 25 or more than 25 PRBs, then the user is considered to be a cell-centre user, otherwise it is classified as a cell-edge user. For the analytical CP_r computation, (11) and (15) are used for the independent and correlated cases, respectively. Fig. 4 shows the variation of CP_r as a function of the SINR threshold for FR1, FR3, and the FFR case using both our analytical expressions in (11) and (15) and simulations. Observe in Fig. 4 that the analytical results match the simulation results. It can be seen that for the independent fading case, the CP_r reaches its maximum, when $S_{th} = T$ and it becomes higher than the FR3 CP_r. However, for the fully correlated case, the CP_r becomes maximum, when $S_{th} \geq T$ and it is equal to the FR3 CP_r.

Note that all our results are based on considering Rayleigh fading. However, the results seem to be valid for general fading. For example, Fig. 5 shows the variation of CP_r as a function of the SINR threshold by considering Nakagami-m fading using simulations. The CP_r is shown for the FR1, FR3 and FFR scenarios for the different values of the Nakagami shape parameter m. Similar to the Rayleigh fading scenario, the CP_r reaches its maximum, when $S_{th} = T$ and it becomes higher than the FR3 CP_r. Interestingly, as the Nakagami shape parameter increases, the gap between the optimal FFR CP_r and FR3 CP_r

IEEE Proof

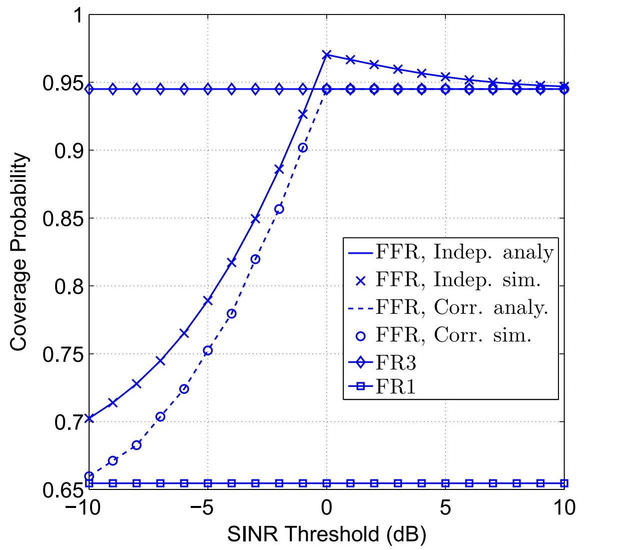

Fig. 4. Coverage probability of FR1, FR3 and FFR evaluated for (11) and (15) with respect to SINR Threshold S_{th}. Here, $T = 0$ dB, $\alpha = 3.2$ and $N_t = N_r = 1$.

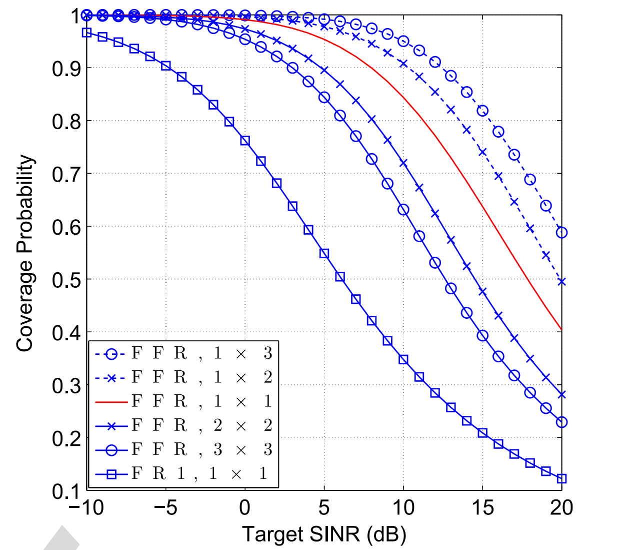

Fig. 6. Coverage probability of both FR1 and of FFR-aided MU-MIMO and SIMO case evaluated for (11) versus the target SINR T. Here we have $\alpha = 4$ and $S_{th} = T$ dB, $\delta = 3$.

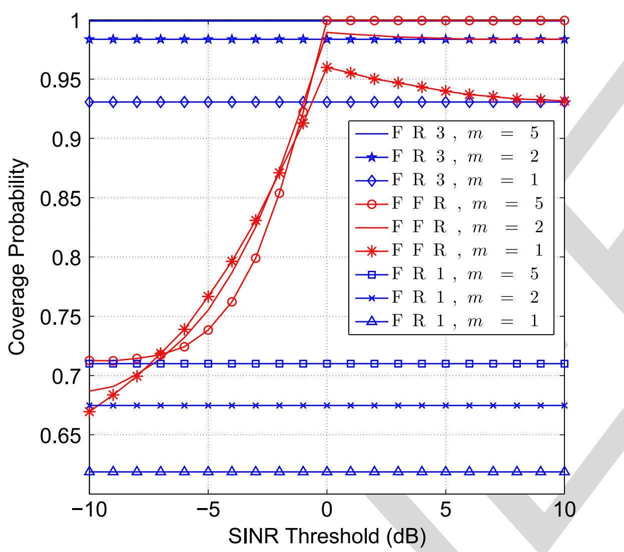

Fig. 5. Coverage probability of FR1, FR3 and FFR for different value of shape parameter for Nakagami-m fading. Here, $T = 0$ dB, $\alpha = 3$ and $N_t = N_r = 1$.

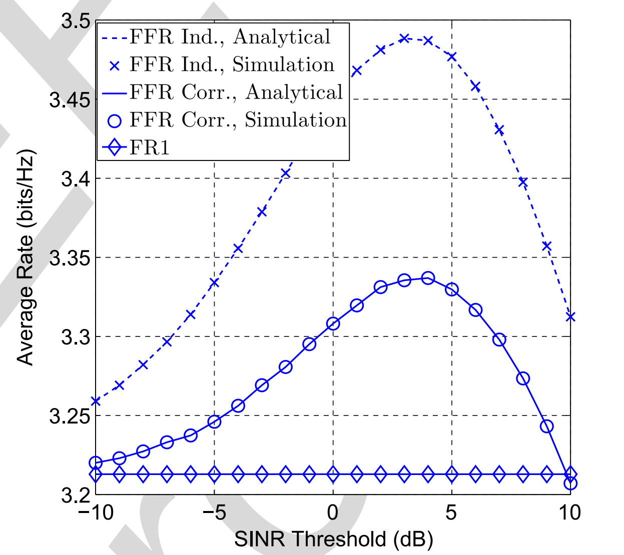

Fig. 7. Average rate of FR1 and FFR versus the SINR threshold. Here we have $\alpha = 4$, $N_t = N_r = 1$. The theoretical results are plotted from Eq. (26) and (34).

decreases and it almost becomes negligible, when the shape parameter is in excess of $m = 5$.

Fig. 6 depicts the CP_r of the FFR-aided MU-MIMO and SIMO systems at the optimal value of S_{th} with respect to the target SINR. The CP_r of FR1 is also plotted for reference. It can be observed in Fig. 6 that the FR1 CP_r is significantly lower than that of FFR-aided MU-MIMO. The CP_r of the FFR-aided SIMO case is higher than that of the FFR-aided MU-MIMO scenario.

Fig. 7 plots the average rate of both the FFR and FR1 systems versus the SINR threshold. For plotting the analytical result, (26) and (34) are used for the independent and correlated case, respectively. Observe that the simulation results closely match the analytical results. Firstly, it can be seen that the FFR achieves the maximum value of the average rate at 3.3 dB, which is the $S_{opt,R}$ value, as shown in Fig. 3 for a (1×1)-antenna system. Secondly, it can be observed in Fig. 7 that the average rate is reduced, when the sub-bands are correlated. Furthermore, interestingly, the optimal SINR threshold of the correlated case is nearly the same as the optimal SINR threshold of the independent fading case. Although, we have considered continuous log-shaped curve mapping between the SINR and the data rate, in practical scenarios, the mapping is given by discrete curves asscociated with different modulation and coding schemes (MCSs). Therefore, we have also provided the average rate versus the SINR threshold based on the specific MCS level using simulation results as shown in Fig. 8. The mapping between SINR and data rate is based on Table 10.1 of the [34]. It can be observed that the value of $S_{opt,R}$ is the same as observed in Fig. 7. Furthermore, the optimal SINR threshold of the correlated case is nearly the same as the optimal SINR threshold of the independent fading scenario.

IEEE Proof

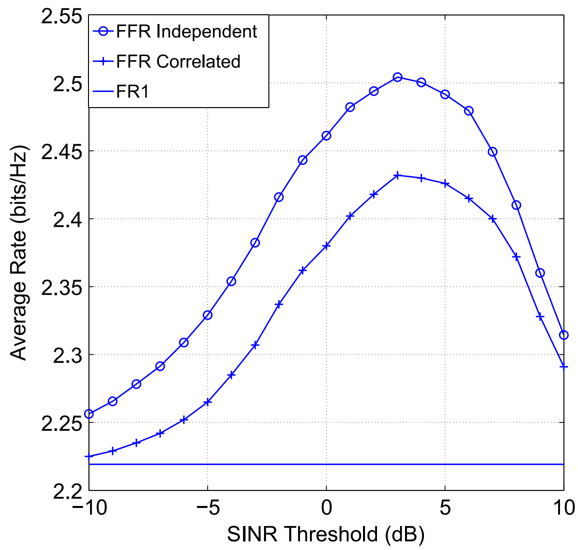

Fig. 8. Average rate of FR1 and FFR using MCS labels versus the SINR threshold. Here we have $\alpha = 4$, $N_t = N_r = 1$.

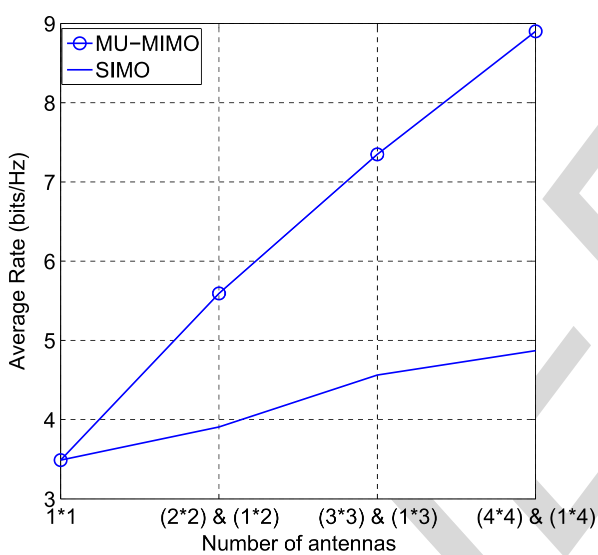

Fig. 9. Maximum average rate achieved by the FFR-aided MU-MIMO and SIMO systems evaluated using (26) and (27) versus the number of antennas for $\alpha = 4$.

Let us now compare the average rate achieved by the MU-MIMO and SIMO scenarios at the optimal SINR thresholds. Fig. 9 plots the average rate achieved by the MU-MIMO and SIMO scenarios versus the number of antennas. It is interesting to note that the average rate achieved by the MU-MIMO case is significantly higher than that of the SIMO case. For example, the average rate achieved by the (2×2) MU-MIMO case and by the (1×3) SIMO case are 5.6 bits/Hz and 4.56 bits/Hz, respectively. In other words, the (2×2) MU-MIMO system achieves a 22.5% higher rate than the (1×3) SIMO system. However, the overall CP_r achieved by the SIMO case is higher than that of the MU-MIMO case. Now a natural question arises, which of the systems should be chosen by the system designer, since both the CP_r as well as the average rate are important metrics. Based on our results, system designer may opt for the (2×2) MU-MIMO system over the (1×3) SIMO system, since the gain in average rate is significant and the CP_r degradation for (2×2) MU-MIMO is low for lower target SINRs.

Finally, we have two different expressions for optimal SINR threshold for both the cases, one corresponding to CP_r $(S_{th} = T)$ and other corresponding to average rate $(S_{th} = T')$. To maximize both CP_r as well as average rate simultaneously, the system designer would have to choose one of these two expressions. Now the question arises as to which expression is more appropriate? In order to answer this, we first discuss the benefit of FFR. We see from Figs. 3 and 4 that FFR provides 48% gain in CP_r and 8.5% gain in average rate with respect to FR1 at the optimal S_{th}. In other words, FFR provides significantly high gain in CP_r and hence this scheme would be more useful when coverage gain is essentially required. Therefore, FFR-aided MU-MIMO provides both high average rate and satisfactory CP_r, since due to MU-MIMO average rate is high and due to FFR scheme CP_r is satisfactory. It can be also noted from Fig. 4 that when S_{th} is higher than the optimal S_{th}, the loss in CP_r is negligible, while when S_{th} is lower than the optimal S_{th}, there is significant change in CP_r. Hence, for the lower target SINR scenario, i.e., $T < T'$, the system designer should choose optimal S_{th} corresponding to average rate $(S_{th} = T')$. On the other hand, for higher target SINR scenario, i.e., $T > T'$, the system designer should choose optimal S_{th} corresponding to CP_r $(S_{th} = T)$.

VI. Conclusion

We have derived expressions for both the CP_r and average rate of MU-MIMO and SIMO systems based on a planned FFR deployment. The impact of frequency-domain correlation between the sub-bands allocated to the FR1 and FR3 regions on the average rate and on the CP_r was analysed in detail, since any practical OFDMA system will typically experience frequency-domain correlation. We analytically determined the optimal SINR threshold, which maximizes the CP_r, and also determined the optimal SINR threshold (denoted by $S_{opt,R}$), which maximizes the average rate for both the MU-MIMO and SIMO systems considered. It was shown that for the optimal choice of the SINR threshold, the CP_r of the FFR system is higher than that of its FR3 counterpart. The value of $S_{opt,R}$ increases, when the number of antennas is reduced in a MU-MIMO, where it is assumed that the number of transmit antennas is equal to the number of receive antennas, i.e., $N_t = N_r = N_a$. However, it increases when the number of receive antennas increases in the SIMO scenario. Furthermore, the performance of FFR of the MU-MIMO system and SIMO system are compared. It was shown that $(N_a \times N_a)$-element FFR-aided MU-MIMO achieves a significantly higher average rate than $(1 \times 2N_a - 1)$-element SIMO counterpart, but MU-MIMO achieves a lower coverage quality than its SIMO counterpart. However its average rate improvement is more significant than its CP_r reduction, especially for a lower value of N_a and for a lower target SINR. Hence a (2×2) system is preferred over a (1×3) system.

A natural extension of this work is to study the FFR-aided MU-MIMO and SIMO system in the context of the cellular uplink [35], [36]. In this study, we have assumed having a fixed transmission power and that the resource blocks are

IEEE Proof

equitably shared by the users. Our future work could consider unequal transmit powers and the unequal allocation of the resource blocks as well as the study of both FFR-aided MU-MIMO and SIMO systems. Moreover, although strict FFR was considered in the paper, it would also be of substantial interest to study dynamic FFR-aided MU-MIMO and SIMO systems.

Appendix A

To obtain the $S_{opt,C}$, we consider the following three possibilities: (*i*) $S_{th} < T$, (*ii*) $S_{th} = T$, (*iii*) $S_{th} > T$.

(i) $S_{th} < T$: Let $S_{th} = T - \Delta$, where $\Delta > 0$, then $P_f(r)$ can be expressed as in terms of T

$$P_F(r, S_{th} < T) = \prod_{i\in\psi}\left(\frac{1}{1+Tr^{\alpha}d_i^{-\alpha}}\right)^{N_t} e^{-Tr^{\alpha}\frac{\sigma^2}{P}} + P_3(T,r) - P_3(T,r)P_1(T-\Delta,r). \quad (35)$$

(ii) $S_{th} = T$: In this case $P_f(r)$ in terms of T can be formulated as

$$P_F(r, S_{th} = T) = \prod_{i\in\psi}\left(\frac{1}{1+Tr^{\alpha}d_i^{-\alpha}}\right)^{N_t} e^{-Tr^{\alpha}\frac{\sigma^2}{P}} + P_3(T,r) - P_3(T,r)P_1(T,r). \quad (36)$$
$$= P_1(T,r)\left(1 - P_3(T,r)\right) + P_3(T,r). \quad (37)$$

(iii) $S_{th} > T$: Let $S_{th} = T + \Delta$, where $\Delta > 0$, then $P_f(r)$ in terms of T is given by

$$P_F(r, S_{th} > T) = \prod_{i\in\psi}\left(\frac{1}{1+(T+\Delta)r^{\alpha}d_i^{-\alpha}}\right)^{N_t} e^{-(T+\Delta)r^{\alpha}\frac{\sigma^2}{P}} + P_3(T,r) - P_3(T,r)P_1(T+\Delta,r).$$
$$= P_1(T+\Delta,r)\left(1 - P_3(T,r)\right) + P_3(T,r). \quad (38)$$

Let us now compare the FFR CP_r for $S_{th} < T$ and $S_{th} = T$ given by (35) and (36), respectively. Since we have $P_1(T-\Delta, r) > P_1(T,r)$, this implies that $P_F(r, S_{th} < T) < P_F(r, S_{th} = T)$. Similarly, we compare the FFR-aided CP_r for $S_{th} = T$ and $S_{th} > T$ given by (37) and (38), respectively. Since $P_1(T+\Delta, r) < P_1(T,r)$, this implies that $P_F(r, S_{th} = T) > P_F(r, S_{th} > T)$. Thus, FFR achieves the maximum achievable CP_r when $S_{th} = T$. Note that when one chooses the SINR threshold to be $S_{opt,C}$, then the CP_r of FFR is higher than that of FR3 since we have $CP_F(r, S_{th} = T) = P_1(T,r)(1 - P_3(T,r)) + P_3(T,r) > P_3(T,r)$. The reason for this behaviour is as follows: only users having a low SINR (low fading gain for the desired signal and/or high fading gain for the interfering signal) move to the cell-edge region and they experience a new independent fading gain at the cell-edge region. In other words, the increase in FFR CP_r over the FR3 CP_r is due to the sub-band diversity gains which is achieved by the system, when the users move from the cell-centre to the cell-edge.

Appendix B

Since a cell-centre user is associated with $\eta_t(r) > S_{th}$, the average rate $R_c(r)$ of the cell-centre users of the FFR system can be written as $R_c(r) = E[\ln(1+\eta_t(r))|\eta_t(r) > S_{th}]$ Similarly, since a cell-edge user has $\eta_t(r) < S_{th}$, the average rate $R_e(r)$ of the cell-edge users in the FFR system can be written as $R_e(r) = E[\ln(1+\hat{\eta}_t(r))|\eta_t(r) < S_{th}]$. Now, the average rate $R_f(r)$ of the FFR system can be written as

$$R_f(r) = R_c(r)P\left[\eta_t(r) > S_{th}\right] + \frac{1}{3}R_e(r)P\left[\eta_t(r) < S_{th}\right]. \quad (39)$$

Here the first term denotes the average rate contributed by the cell-centre users, while the second term denotes the contribution of the cell-edge users. Recall that the frequency reuse $\frac{1}{3}$ is invoked for the cell-edge users. In other words, only one third of the cell-edge frequency $(F_1 + F_2 + F_3)$ is used for the cell-edge users and hence the factor $\frac{1}{3}$ is multiplied in the above expression. Using the methods outlined in Section IV-A, $R_c(r)P[\eta(r) > S_{th}]$ can be written as

$$R_c(r)P\left[\eta_t(r) > S_{th}\right] = \int_{t>0} P\left[\ln(1+\eta_t(r)) > t,\, \eta_t)r) > S_{th}\right] \mathrm{d}t$$
$$= \int_{t>0} P\left[\eta_t(r) > \max\{e^t - 1, S_{th}\}\right] \mathrm{d}t. \quad (40)$$

Using (3) and (4), this can be further simplified to

$$R_c(r)P\left[\eta_t(r) > S_{th}\right] = \int_{t>0}\prod_{j\in\psi}\left(\frac{1}{1+\max\{e^t-1, S_{th}\}r^{\alpha}d_j^{-\alpha}}\right)^{N_t} \mathrm{d}t. \quad (41)$$

Again, similar to Section IV-A, we can write $R_e(r)$ as

$$R_e(r) = \int_{t>0}\frac{P\left[\ln\left(1+\hat{\eta}_t(r)\right) > t,\, \eta_t(r) < S_{th}\right]}{P\left[\eta_t(r) < S_{th}\right]}\mathrm{d}t$$
$$= \int_{t>0}\frac{P\left[\hat{\eta}_t(r) > (e^t-1),\, \eta_t(r) < S_{th}\right]}{P\left[\eta_t(r) < S_{th}\right]}\mathrm{d}t. \quad (42)$$

Since g and $\hat{g}$ are i.i.d as well as h_i and $\hat{h}_i$ are also i.i.d, hence $R_e(r)$ can be written as

$$R_e(r) = \int_{t>0}\prod_{i\in\phi}\left(\frac{1}{1+(e^t-1)r^{\alpha}d_i^{-\alpha}}\right)^{N_t} \mathrm{d}t. \quad (43)$$

Finally substituting back (41) and (43) into (39) and after averaging over the spatial dimension, the average rate of the FFR system is given by

$$R_f = \int_0^R\int_{t>0}\left(\prod_{j\in\psi}\left(\frac{1}{1+\max\{e^t-1, S_{th}\}r^{\alpha}d_j^{-\alpha}}\right)^{N_t} + \frac{1}{3}\prod_{i\in\phi}\frac{P\left[\eta_t(r) < S_{th}\right]}{\left(1+(e^t-1)r^{\alpha}d_i^{-\alpha}\right)^{N_t}}\right)\mathrm{d}t f_R(r)\mathrm{d}r. \quad (44)$$

IEEE Proof

APPENDIX C

The average rate expression can be written as

$$R_f = \int_0^R \int_{t>0} \left(\prod_{j\in\psi} \left(\frac{1}{1+\max\{e^t-1, S_{th}\} r^\alpha d_j^{-\alpha}} \right)^{N_t} + \frac{1}{3} \prod_{i\in\phi} \frac{P[\eta_t(r) < S_{th}]}{\left(1+(e^t-1) r^\alpha d_i^{-\alpha}\right)^{N_t}} \right) \mathrm{d}t f_R(r) \mathrm{d}r. \quad (45)$$

To maximize the rate R_f, we have to differentiate R_f with respect to S_{th}. In order to do that we split the first part of the integrand of R_f as given in (46), shown at the bottom of the page. Upon substituting $P[\eta_t(r) < S_{th}] = 1 - \prod_{j\in\psi} \left(\frac{1}{1+S_{th} r^\alpha d_j^{-\alpha}} \right)^{N_t}$ into Eq. (45), R_f can be rewritten as given in (47), shown at the bottom of the page. Using Leibniz's rule,[6] while differentiating R_f with respect to S_{th}, we obtain (48), shown at the bottom of the page. Simplifying $\frac{dR_f}{dS_{th}}$ and equating it to zero, one obtains $\frac{dR_f}{dS_{th}}$ as given in (48). The solution of the integral given in (48) gives the optimal S_{th}, namely $S_{opt,R}$, but obtaining $S_{opt,R}$ in a closed form is a challenging problem, as the distances d_is are also a function of r. Hence, we find the value of $S_{opt,R}$ by solving (48) numerically (using Mathematica (or Matlab)). Note that the optimal value of S_{th} is calculated at the time of network planning with the aid of Mathematica (or Matlab) to obtain the numerical values off line. We have investigated $S_{opt,R}$ as a function of the path loss exponent, of the number of transmit antennas, etc.

[6] Leibniz's rule states that if $f(x, \theta)$ is a function such that $\frac{d}{d\theta} f(x, \theta)$ exist, and it is continuous, then we have $\frac{d}{d\theta} \left(\int_{a(\theta)}^{b(\theta)} f(x, \theta)\, dx \right) = \int_{a(\theta)}^{b(\theta)} \frac{d}{d\theta} (f(x, \theta))\, dx + f(b(\theta), \theta) \frac{d}{d\theta} b(\theta) - f(a(\theta), \theta) \frac{d}{d\theta} a(\theta)$.

$$\int_{t>0} \prod_{j\in\psi} \left(\frac{1}{1+\max\{e^t-1, S_{th}\} r^\alpha d_j^{-\alpha}} \right)^{N_t} \mathrm{d}t = \int_{t>0}^{\ln(1+S_{th})} \prod_{j\in\psi} \left(\frac{1}{1+S_{th} r^\alpha d_j^{-\alpha}} \right)^{N_t} \mathrm{d}t + \int_{\ln(1+S_{th})}^{\infty} \prod_{j\in\psi} \left(\frac{1}{1+(e^t-1) r^\alpha d_j^{-\alpha}} \right)^{N_t} \mathrm{d}t \quad (46)$$

$$R_f = \int_0^R \left(\prod_{j\in\psi} \frac{\ln(1+S_{th})}{\left(1+S_{th} r^\alpha d_j^{-\alpha}\right)^{N_t}} + \int_{\ln(1+S_{th})}^{\infty} \prod_{j\in\psi} \left(\frac{1}{1+(e^t-1) r^\alpha d_j^{-\alpha}} \right)^{N_t} \mathrm{d}t + \left(1 - \prod_{j\in\psi} \left(\frac{1}{1+S_{th} r^\alpha d_j^{-\alpha}} \right)^{N_t} \right) \underbrace{\frac{1}{3} \int_{t>0} \prod_{i\in\phi} \left(\frac{1}{1+(e^t-1) r^\alpha d_i^{-\alpha}} \right)^{N_t} \mathrm{d}t}_{K(r)} \right) f_R(r) \mathrm{d}r. \quad (47)$$

$$\frac{dR_f}{dS_{th}} = \int_0^R \left(\frac{ \frac{\prod_{j\in\psi} \left(1+S_{th} r^\alpha d_j^{-\alpha}\right)^{N_t}}{1+S_{th}} - \ln(1+S_{th}) \frac{d}{dS_{th}} \left(\prod_{j\in\psi} \left(1+S_{th} r^\alpha d_j^{-\alpha}\right)^{N_t} \right) }{ \left(\prod_{j\in\psi} \left(1+S_{th} r^\alpha d_j^{-\alpha}\right) \right)^{2N_t} } - \prod_{j\in\psi} \frac{1}{\left(1+S_{th} r^\alpha d_j^{-\alpha}\right)^{N_t}} \left(\frac{1}{1+S_{th}} \right) + \frac{ K(r) \frac{d}{dS_{th}} \left(\prod_{j\in\psi} \left(1+S_{th} r^\alpha d_j^{-\alpha}\right)^{N_t} \right) }{ \left(\prod_{j\in\psi} \left(1+S_{th} r^\alpha d_j^{-\alpha}\right) \right)^{2N_t} } \right) f_R(r) \mathrm{d}r.$$

$$\frac{dR_f}{dS_{th}} = \int_0^R \left(\frac{ (K(r) - \ln(1+S_{th})) \sum_{i\in\psi} \left(1+S_{th} r^\alpha d_i^{-\alpha}\right)^{N_t-1} r^\alpha d_i^{-\alpha} \left(\prod_{j\in\psi\setminus i} \left(1+S_{th} r^\alpha d_j^{-\alpha}\right)^{N_t} \right) }{ \left(\prod_{j\in\psi} \left(1+S_{th} r^\alpha d_j^{-\alpha}\right) \right)^{2N_t} } \right) f_R(r) \mathrm{d}r = 0 \quad (48)$$

IEEE Proof

References

[1] G. Boudreau *et al.*, "Interference coordination and cancellation for 4G networks," *IEEE Commun. Mag.*, vol. 47, no. 4, pp. 74–81, Apr. 2009.

[2] N. Himayat, S. Talwar, A. Rao, and R. Soni, "Interference management for 4G cellular standards [WIMAX/LTE UPDATE]," *IEEE Commun. Mag.*, vol. 48, no. 8, pp. 86–92, Aug. 2010.

[3] F. Wang *et al.*, "Mobile WiMAX systems: Performance and evolution," *IEEE Commun. Mag.*, vol. 46, no. 10, pp. 41–49, Oct. 2008.

[4] D. Astely *et al.*, "LTE: The evolution of mobile broadband," *IEEE Commun. Mag.*, vol. 47, no. 4, pp. 44–51, Apr. 2009.

[5] A. S. Hamza, S. S. Khalifa, H. S. Hamza, and K. Elsayed, "A survey on inter-cell interference coordination techniques in OFDMA-based cellular networks," *IEEE Commun. Surveys Tuts.*, vol. 15, no. 4, pp. 1642–1670, 4th Quart. 2013.

[6] R. Y. Chang, Z. Tao, J. Zhang, and C.-C. J. Kuo, "A graph approach to dynamic Fractional Frequency Reuse (FFR) in multi-cell OFDMA networks," in *Proc. IEEE ICC*, Jun. 2009, pp. 1–6.

[7] M. Assaad, "Optimal Fractional Frequency Reuse (FFR) in multicellular OFDMA system," in *Proc. IEEE 68th VTC-Fall*, Sep. 2008, pp. 1–5.

[8] Z. Xu, G. Ye Li, C. Yang, and X. Zhu, "Throughput and optimal threshold for FFR schemes in OFDMA cellular networks," *IEEE Trans. Wireless Commun.*, vol. 11, no. 8, pp. 2776–2785, Aug. 2012.

[9] T. Novlan, J. G. Andrews, I. Sohn, R. K. Ganti, and A. Ghosh, "Comparison of fractional frequency reuse approaches in the OFDMA cellular downlink," in *Proc. IEEE Global Telecommun. Conf.*, 2010, pp. 1–5.

[10] T. D. Novlan, R. K. Ganti, A. Ghosh, and J. G. Andrews, "Analytical evaluation of fractional frequency reuse for OFDMA cellular networks," *IEEE Trans. Wireless Commun.*, vol. 10, no. 12, pp. 4294–4305, Dec. 2011.

[11] H. Zhuang and T. Ohtsuki, "A model based on Poisson point process for analyzing MIMO heterogeneous networks utilizing fractional frequency reuse," *IEEE Trans. Wireless Commun.*, vol. 13, no. 12, pp. 6839–6850, Dec. 2014.

[12] A. Mahmud and K. A. Hamdi, "A unified framework for the analysis of fractional frequency reuse techniques," *IEEE Trans. Commun.*, vol. 62, no. 10, pp. 3692–3705, Oct. 2014.

[13] D. G. Gonzalez, M. Garcia-Lozano, S. Ruiz Boque, and D. S. Lee, "Optimization of soft frequency reuse for irregular LTE macrocellular networks," *IEEE Trans. Wireless Commun.*, vol. 12, no. 5, pp. 2410–2423, May 2013.

[14] X. Tao, F. Xu, W. ur Rehman, Y. Xu, and X. Li, "A generic mathematical model based on fuzzy set theory for frequency reuse in cellular networks," *IEEE J. Sel. Areas Commun.*, vol. 31, no. 5, pp. 861–869, May 2013.

[15] L.-C. Wang and C.-J. Yeh, "3-cell network MIMO architectures with sectorization and fractional frequency reuse," *IEEE J. Sel. Areas Commun.*, vol. 29, no. 6, pp. 1185–1199, Jun. 2011.

[16] S. Kumar and S. Kalyani, "Impact of correlated interferers on coverage and rate of FFR and SFR schemes," *IEEE Trans. Veh. Technol.*, to be published. AQ3

[17] H. Chang and I. Rubin, "Optimal downlink and uplink fractional frequency reuse in cellular wireless networks" *IEEE Trans. Veh. Technol.*, to be published. AQ4

[18] O. Aliu, M. Mehta, M. Imran, A. Karandikar, and B. Evans, "A new cellular-automata-based fractional frequency reuse scheme," *IEEE Trans. Veh. Technol.*, vol. 64, no. 4, pp. 1535–1547, Apr. 2015.

[19] Q. Li, R. Hu, Y. Xu, and Y. Qian, "Optimal fractional frequency reuse and power control in the heterogeneous wireless networks," *IEEE Trans. Wireless Commun.*, vol. 12, no. 6, pp. 2658–2668, Jun. 2013.

[20] J. Zhang, R. Zhang, G. Li, and L. Hanzo, "Distributed antenna systems in fractional-frequency-reuse-aided cellular networks," *IEEE Trans. Veh. Technol.*, vol. 62, no. 3, pp. 1340–1349, Mar. 2013.

[21] S. Kumar, S. Kalyani, and K. Giridhar, "Spectrum allocation for ICIC based picocell," *IEEE Trans. Veh. Technol.*, to be published. AQ5

[22] F. Jin, R. Zhang, and L. Hanzo, "Fractional frequency reuse aided twin-layer femtocell networks: Analysis, design and optimization," *IEEE Trans. Commun.*, vol. 61, no. 5, pp. 2074–2085, May 2013.

[23] W. S. Jeon, J. Kim, and D. G. Jeong, "Downlink radio resource partitioning with fractional frequency reuse in femtocell networks," *IEEE Trans. Veh. Technol.*, vol. 63, no. 1, pp. 308–321, Jan. 2014.

[24] F. Wang and W. Wang, "Analytical evaluation of femtocell deployment in cellular networks using fractional frequency reuse," *IET Commun.*, vol. 8, no. 9, pp. 1599–1608, Jun. 2014.

[25] N. Saquib, E. Hossain, and D. I. Kim, "Fractional frequency reuse for interference management in lte-advanced hetnets," *IEEE Wireless Commun.*, vol. 20, no. 2, pp. 113–122, Apr. 2013.

[26] J. Y. Lee, S. J. Bae, Y. M. Kwon, and M. Y. Chung, "Interference analysis for femtocell deployment in OFDMA systems based on fractional frequency reuse," *IEEE Commun. Lett.*, vol. 15, no. 4, pp. 425–427, Apr. 2011.

[27] Q. H. Spencer, A. L. Swindlehurst, and M. Haardt, "Zero-forcing methods for downlink spatial multiplexing in multiuser MIMO channels," *IEEE Trans. Signal Process.*, vol. 52, no. 2, pp. 461–471, Feb. 2004.

[28] D. Gesbert, M. Kountouris, R. W. Heath, C.-B. Chae, and T. Salzer, "Shifting the MIMO paradigm," *IEEE Signal Process. Mag.*, vol. 24, no. 5, pp. 36–46, Sep. 2007.

[29] S. Jafar and A. Goldsmith, "Isotropic fading vector broadcast channels: The scalar upper bound and loss in degrees of freedom," *IEEE Trans. Inf. Theory*, vol. 51, no. 3, pp. 848–857, Mar. 2005.

[30] S. Catreux, P. Driessen, and L. Greenstein, "Simulation results for an interference-limited multiple-input multiple-output cellular system," *IEEE Commun. Lett.*, vol. 4, no. 11, pp. 334–336, Nov. 2000.

[31] J. G. Andrews, W. Choi, and R. W. Heath, "Overcoming interference in spatial multiplexing MIMO cellular networks," *IEEE Wireless Commun.*, vol. 14, no. 6, pp. 95–104, Dec. 2007.

[32] D. Tse and P. Viswanath, *Fundamentals of Wireless Communication*. Cambridge, U.K.: Cambridge Univ. Press, 2005.

[33] K. B. Baltzis, "Hexagonal vs circular cell shape: A comparative analysis and evaluation of the two popular modeling approximations," in *Cellular Networks-Positioning, Performance Analysis, Reliability*, A. Melikov Ed. Rijeka, Croatia: Intechopen, 2011. AQ6

[34] S. Sesia, I. Toufik, and M. Baker, *LTE-The UMTS Long Term Evolution: From Theory to Practice*. Hoboken, NJ, USA: Wiley, 2011. [Online]. Available: https://books.google.co.uk/books?id=beIaPXLzYKcC

[35] H. Tabassum, F. Yilmaz, Z. Dawy, and M.-S. Alouini, "A framework for uplink intercell interference modeling with channel-based scheduling," *IEEE Trans. Wireless Commun.*, vol. 12, no. 1, pp. 206–217, Jan. 2013.

[36] H. Tabassum, Z. Dawy, M. S. Alouini, and F. Yilmaz, "A generic interference model for uplink OFDMA networks with fractional frequency reuse," *IEEE Trans. Veh. Technol.*, vol. 63, no. 3, pp. 1491–1497, Mar. 2014.

Suman Kumar received the B.Tech. degree in electronics and communication engineering from the Future Institute of Engineering and Management, Kolkata, India, in 2010. He is currently pursuing the Ph.D. degree in the Department of Electrical Engineering, Indian Institute of Technology, Madras, India. He is the recipient of a Best Paper Award at ICWMC-2012 held at Venice, Italy.

His research interests are broadly in the areas of performance analysis of mobile broadband wireless networks including frequency reuse, HetNets, hypergeometric functions, and generalized fading models.

Sheetal Kalyani received the B.E. degree in electronics and communication engineering from the Sardar Patel University, Gujarat, India, in 2002 and the Ph.D. degree in electrical engineering from the Indian Institute of Technology, Madras, India, in 2008. She was a Senior Research Engineer in Centre of Excellence in Wireless Technology, Chennai, India, from 2008 to 2012. She is currently an Assistant Professor in the Department of Electrical Engineering, Indian Institute of Technology, Madras.

Her current research interests include HetNets, extreme value theory, hypergeometric functions, generalized fading models, and statistical learning algorithms for prediction.

IEEE Proof

Lajos Hanzo (M'91–SM'92–F'04) received the degree in electronics in 1976 and his doctorate in 1983 from the Technical University of Budapest, Budapest, Hungary. In 2009, he was awarded an honorary doctorate by the Technical University of Budapest, and in 2015 by the University of Edinburgh. During his 38-year career in telecommunications, he has held various research and academic posts in Hungary, Germany, and the U.K. Since 1986, he has been with the School of Electronics and Computer Science, University of Southampton, U.K., where he holds the Chair in telecommunications. He has successfully supervised about 100 Ph.D. students, co-authored 20 John Wiley/IEEE Press books on mobile radio communications totalling in excess of 10 000 pages, published over 1500 research entries at IEEE Xplore, acted both as TPC and General Chair of IEEE conferences, presented keynote lectures, and been awarded a number of distinctions. Currently, he is directing a 60-strong academic research team, working on a range of research projects in the field of wireless multimedia communications sponsored by industry, the Engineering and Physical Sciences Research Council (EPSRC) U.K., the European Research Council's Advanced Fellow Grant, and the Royal Society's Wolfson Research Merit Award. He is an enthusiastic supporter of industrial and academic liaison and he offers a range of industrial courses. He is also a Governor of the IEEE Vehicular Technology Society. During 2008–2012, he was the Editor-in-Chief of the IEEE Press and a Chaired Professor also at Tsinghua University, Beijing. His research is funded by the European Research Council's Senior Research Fellow Grant. Dr. Hanzo has over 22 000 citations. For further information on research in progress and associated publications, please refer to http://www-mobile.ecs.soton.ac.uk.

K. Giridhar (M'XX) received the B.Sc. degree in applied sciences from PSG College of Technology, Coimbatore, India, the M.E. degree in electrical communications from Indian Institute of Science, Bangalore, India, and the Ph.D. degree in electrical engineering from University of California, Santa Barbara, Santa Barbara, CA, USA. AQ7

He is a Professor at the Indian Institute of Technology Madras (www.iitm.ac.in), Chennai. During 1989 and 1990, he was a Member of Research Staff at CRL, Bharat Electronics, Bangalore, and during 1993 and 1994, was a Research Affiliate in electrical engineering at Stanford University, Stanford, CA, USA. Since 1994, he has been with the Department of Electrical Engineering, Indian Institute of Technology, Madras (ITTM). He has been a Visiting Faculty at Sri Sathya Sai Institute of Higher Learning, Prasanthi Nilayam, Andhra Pradesh, and at Stanford University. His research interests are broadly in the areas of adaptive signal processing and wireless communications systems, with an emphasis on various transceiver algorithms, custom air-interface design for strategic applications, and performance analysis of mobile broadband wireless networks including HetNets.

Dr. Giridhar is a member of the Telecommunications and Computer Networks (TeNeT) Group (www.tenet.res.in) at IITM. He actively collaborates with the Center of Excellence in Wireless Technology (www.cewit.org.in) on MIMO-OFDM broadband access research, resulting in several contributions to IEEE 802.16m, and currently on proposals to LTE-A and 5G forums. He serves as a consultant to many telecom & VLSI companies in India, and was on a sabbatical in 2004–2005 with Beceem Communications.

IEEE Proof

AUTHOR QUERIES

AUTHOR PLEASE ANSWER ALL QUERIES

AQ1 = Please provide keywords.
AQ2 = Please provide department name for IIT, Madras.
AQ3 = Please provide publication update in Ref. [16].
AQ4 = Please provide publication update in Ref. [17].
AQ5 = Please provide publication update in Ref. [21].
AQ6 = Please provide page range of chapter for Ref. [33].
AQ7 = Please provide membership history for K. Giridhar.

END OF ALL QUERIES

IEEE Proof

Coverage Probability and Achievable Rate Analysis of FFR-Aided Multi-User OFDM-Based MIMO and SIMO Systems

Suman Kumar, Sheetal Kalyani, Lajos Hanzo, *Fellow, IEEE*, and K. Giridhar, *Member, IEEE*

***Abstract*—Expressions are derived for the coverage probability and average rate of both multi-user multiple input multiple output (MU-MIMO) and single input multiple output (SIMO) systems in the context of a fractional frequency reuse (FFR) scheme. In particular, given a reuse region of $\frac{1}{3}$ (FR3) and a reuse region of 1 (FR1) as well as a signal-to-interference-plus-noise-ratio (SINR) threshold S_{th}, which decides the user assignment to either the FR1 or FR3 regions, we theoretically show that: 1) the optimal choice of S_{th} which maximizes the coverage probability is $S_{th} = T$, where T is the target SINR required for ensuring adequate coverage, and 2) the optimal choice of S_{th} which maximizes the average rate is given by $S_{th} = T'$, where T' is a function of the path loss exponent, the number of antennas and of the fading parameters. The impact of frequency domain correlation amongst the OFDM sub-bands allocated to the FR1 and FR3 cell-regions is analysed and it is shown that the presence of correlation reduces both the coverage probability and the average throughput of the FFR network. Furthermore, the performance of our FFR-aided MU-MIMO and SIMO systems is compared. Our analysis shows that the (2 × 2) MU-MIMO system achieves 22.5% higher rate than the (1 × 3) SIMO system and for lower target SINRs, the coverage probability of a (2 × 2) MU-MIMO system is comparable to a (1 × 3) SIMO system. Hence the former one may be preferred over the latter. Our simulation results closely match the analytical results.**

***Index Terms*—Author, please supply index terms/keywords for your paper. To download the IEEE Taxonomy go to http://www.ieee.org/documents/taxonomy_v101.pdf.**

AQ1

I. Introduction

ORTHOGONAL frequency division multiple access (OFDMA) based systems maintain orthogonality among the intra-cell users, but the radical OFDMA system deployments relying on a frequency reuse factor of unity suffer from inter-cell interference. As a remedy, inter-cell interference coordination (ICIC) schemes have been designed for minimizing the co-channel interference [1]. Fractional frequency reuse (FFR) [2] constitutes a low complexity ICIC scheme, which has been proposed for OFDMA based wireless networks such as IEEE WiMAX [3] and 3GPP LTE [4].

Manuscript received January 18, 2015; revised June 5, 2015; accepted August 1, 2015. The associate editor coordinating the review of this paper and approving it for publication was O. Oyman.

S. Kumar, S. Kalyani, and K. Giridhar are with the Indian Institute of Technology Madras, Chennai 600 036, India (e-mail: ee10d040@ee.iitm.ac.in; skalyani@ee.iitm.ac.in; giri@ee.iitm.ac.in).

AQ2

L. Hanzo is with the School of Electrical and Computer Science, University of Southampton, Southampton SO17 1BJ, U.K. (e-mail: lh@ecs.soton.ac.uk).

Color versions of one or more of the figures in this paper are available online at http://ieeexplore.ieee.org.

Digital Object Identifier 10.1109/TCOMM.2015.2465907

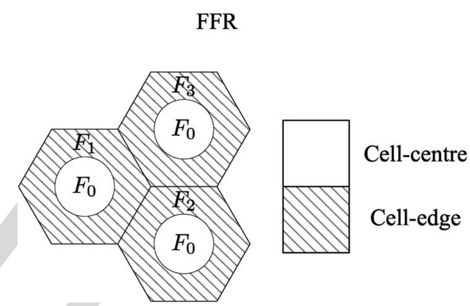

Fig. 1. Frequency allocation in FFR for three neighbouring cells with $\delta = 3$. The cell-centre users of all the cells rely on a common frequency band F_0, while the cell-edge users of the three cells occupy different frequency bands, namely F_1, F_2 and F_3.

Explicitly, FFR is a combination of frequency reuse 1 (FR1) and frequency reuse $\frac{1}{\delta}$ (FRδ). FR1 allocates all the frequencies to each cell, leading to a unity spatial reuse, hence results in a low-quality coverage due to the excessive inter-cell interference. On the other hand, FRδ allocates a fraction of $\frac{1}{\delta}$ of the frequencies to each cell and therefore reduces the area-spectral-efficiency, but improves the SINR. FFR strikes an attractive trade-off by exploiting the advantages of both FR1 and FRδ by relying on FR1 for the cell-centre users i.e. for those users who would experience less interference from the other cells, because they are close to their serving base station (BS). By contrast, FRδ is invoked for the cell-edge users i.e. for those users who would experience high interference afflicted by the co-channel signals emanating from the neighbouring cells in case of FR1, because they are far from their serving BS. Typically, there are two basic modes of FFR deployment: static and dynamic FFR [1]. In this paper, we consider the more practical static FFR scheme, where all the parameters are configured and kept fixed over a certain period of time [5]. Fig. 1 depicts a typical frequency allocation in the context of the FFR scheme for three adjacent cells, where F_1, F_2 and F_3 each use x% of the total spectrum, hence F_0 uses $(100 - 3x)$% of the spectrum.

FFR schemes have been lavishly studied using both system level simulations and theoretical analysis [6]–[11]. The optimization of FFR relying on a distance threshold[1] or SINR threshold[2]

[1]Based on a pre-determined distance from the BS, the subscribers are divided into cell-centre as well as cell-edge users and hence here the design parameter is a distance threshold (R_{th}).

[2]Based on a pre-determined SINR, the subscribers are divided into cell-centre as well as cell-edge users and here the design parameter is the SINR threshold (S_{th}).

0090-6778 © 2015 IEEE. Personal use is permitted, but republication/redistribution requires IEEE permission.
See http://www.ieee.org/publications_standards/publications/rights/index.html for more information.

IEEE Proof

has been studied using graph theory in [6] and convex optimization in [7]. Specifically, it has been shown in [7] that the optimal frequency reuse factor is FR3 for the cell-edge users. The average cell throughput of an FFR system was derived in [8] as a function of the distance threshold. It was shown in [9] that there exists an optimal radius threshold for which the average rate becomes maximum. The performance of FFR and soft frequency reuse (SFR) has been studied in [12] under both fully loaded and partially loaded scenarios. An algorithm was proposed in [13] for enhancing the network capacity and the cell-edge performance for a dynamic SFR deployment relying on realistic irregularly shaped cells. A fuzzy logic based generic model was proposed for deriving different frequency reuse schemes in [14]. As a further development, an FFR based 3-cell network-MIMO based tri-sector BS architecture was presented in [15]. FFR and SFR are compared in the presence of correlated interferers in [16]. The optimal configuration of FFR is determined in [17] for a high-density wireless cellular network. The authors of [18] have proposed a distributed and adaptive solution for interference coordination based on the center of gravity of users in each sector. An optimal FFR and power control scheme which can coordinate the interference among the heterogeneous nodes is proposed in [19].

An analytical framework of calculating both the coverage probability (CP_r) and the average rate of FFR schemes was presented in [10] and [11] for homogeneous single input single output (SISO) and MIMO heterogeneous networks, respectively, using a Poisson point process (PPP). However, the authors of [10], [11] assumed having an unplanned FFR network, where the cells using the same frequency set are randomly allocated. Hence, two cells using the same frequency for the cell-edge users may in fact be co-located [10], [11]. However, in case of FFR based deployments the regions using the same frequency are typically planned to be as far apart as possible and our focus is on these types of deployments. An FFR-aided distributed antenna system (DAS) and an FFR-aided picocell was studied in [20] and [21]. While, an FFR-aided femtocell has been extensively studied in [22]–[26].

However, most of the work based on FFR has considered the conventional SISO case. To the best of our knowledge, no prior work has analytically derived the optimal SINR threshold for FFR, when the number of antennas is high at the transmitter and/or at the receiver. Hence, in this work, we derive both the CP_r and the average achievable rate expressions of FFR in the presence of both MU-MIMO as well as of SIMO systems and derive the optimal SINR threshold corresponding to the desired CP_r and throughput. Furthermore, the performance of FFR-aided MU-MIMOs is compared to that of FFR in the presence of a SIMO system.

The key benefit of MU-MIMO is their ability to improve the spectral efficiency, which has been extensively studied in a single-cell context in the presence of AWGN [27]–[29]. However, it has been shown in [30], [31] with the help of simulation, that the efficiency of MU-MIMOs is significantly eroded in a multi-cell environment due to interference, especially in the cell-edge region. FFR is capable of significantly improving the cell-edge coverage since it uses FR3 for the cell-edge users. Hence we study FFR-aided MU-MIMOs and quantify their average throughput as well as coverage probability.

Furthermore, we carefully examine the correlation of the sub-bands F_0, F_1, F_2 and F_3 in Fig. 1 used in the FFR system considered. All prior work on FFR has assumed that the sub-bands experience independent fading, which is mathematically convenient, but practically not realisable. Indeed, when we consider practical transmission block based modulation such as OFDM, the channel's delay spread is assumed to be confined to the cyclic prefix of the OFDM symbol. Such a limited-duration (typically less than 20% of the useful OFDM symbol duration) impulse response will result in correlation amongst the adjacent frequency domain OFDM sub-channels. More explicitly, unless the sub-bands $F_0 \cdots F_3$ are spaced apart by more than the reciprocal of the delay spread, correlation will exist. Since the delay spread experienced in the downlink is user-dependent, it is virtually impossible to ensure that the sub-bands F_i in Fig. 1 are independent for each user scheduled in the downlink. Therefore, in our analysis we will specifically take into account the correlation of the sub-bands. For FFR-aided MU-MIMO and SIMO systems, the expressions of CP_r and average rate are derived and the following new results are presented:

(a) The optimal SINR threshold that maximizes the CP_r of FFR is derived for a given T. We show that the optimal S_{th} (denoted by $S_{opt,C}$) is $S_{th} = T$ for both the MU-MIMO and SIMO system, and if we choose the SINR threshold to be $S_{opt,C}$, then the achievable CP_r of FFR is higher than that of FR3. The improvement of the FFR CP_r over that of FR3 is due to the resultant sub-band diversity gain achieved by the systems when a user is classified as either a cell-centre or a cell-edge user.

(b) The optimal SINR threshold that maximizes the average rate of FFR is derived. We show that the optimal S_{th} (denoted by $S_{opt,R}$) is equal to T' for both MU-MIMO and SIMO systems, where T' is a fixed SINR value, which depends on the system parameters such as the path loss exponent, the number of antennas, the fading parameters, etc.

(c) The correlation of the sub-bands always degrades both the CP_r and the average rate of the FFR-aided MU-MIMO and SIMO systems.

(d) The performance of FFR-aided MU-MIMO and SIMO systems is compared. It is shown that system designer may choose the (2×2) MU-MIMO system over (1×3) SIMO system of FFR scheme as MU-MIMO achieves significant gain in average rate over SIMO.

We will demonstrate that our analytical results are in close agreement with the simulation results. Moreover, it is shown that at optimal S_{th}, the FFR achieves significantly high gain in CP_r than that of average rate with respect to FR1 and hence this scheme would be more useful when coverage gain is essentially required. Therefore, FFR-aided MU-MIMO provides both high average rate and satisfactory CP_r for a lower value of N_a.

II. System Model

A homogeneous macrocell network relying on hexagonal tessellation and on an inter cell site distance of $2R$ is considered,

IEEE Proof

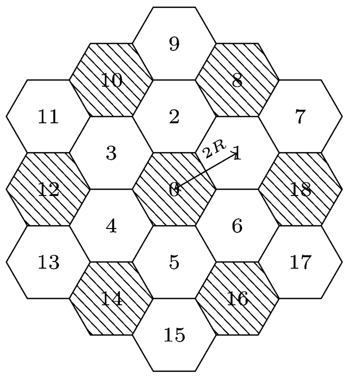

Fig. 2. Hexagonal structure of 2-tier macrocell. Interference for 0th cell in FR1 system is contributed form all the neighbouring 18 cells, while in a FR3 system it is contributed only from the shaded cells.

as shown in Fig. 2. Both a MU-MIMO and a SIMO system is considered. We assume that in the MU-MIMO case each user is equipped with N_r receive antennas, while the BS is equipped with N_t transmit antennas and that $N_t = N_r$. Our focus is on the downlink and hence N_t transmit antennas are used for transmission, while the N_r receive antennas at the UE are used for reception. We also assume that all N_t transmit antennas at the BS are utilized to transmit N_t independent data steams to its own N_t users. A linear minimum mean-square-error (LMMSE) receiver [32] is considered. In order to calculate the post-processing SINR of this LMMSE receiver, it is assumed that the $(N_r - 1)$ closest interferers can be completely cancelled using the antennas at the receiver.[3] For example, in the MU-MIMO case, the user will not experience any intra-tier interference emanating from the serving BS as $N_t = N_r$. In the SIMO case each user is equipped with N_r antennas. The SINR $\eta_t(r)$ of a user in the MU-MIMO system and the SINR $\eta_r(r)$ of a user in the SIMO system located at r meters from its serving BS are given by

$$\eta_t(r) = \frac{g r^{-\alpha}}{\frac{\sigma^2}{P} + I_t}, \quad I_t = \sum_{i \in \psi} \sum_{j=1}^{N_t} h_{ij} d_i^{-\alpha} \tag{1}$$

and

$$\eta_r(r) = \frac{g r^{-\alpha}}{\frac{\sigma^2}{P} + I_r}, \quad I_r = \sum_{i \in \psi_r} h_{ij} d_i^{-\alpha}, \tag{2}$$

respectively, where the transmit power of a BS is denoted by P. Here ψ is the set of interfering BSs in the FR1 network and ψ_r denotes all the interfering BSs, excluding the nearest $(N_r - 1)$ interferers, while N_t denotes the number of transmit antennas. The standard path loss model of $\|x\|^{-\alpha}$ is assumed, where $\alpha \geq 2$ is the path loss exponent and $\|x\|$ is the distance of a user from the BS. We assumed that the users are at least at a distance of d away from the BS.[4] The noise power is denoted by σ^2. Here, r and d_i are the distances from the user to the serving BS and to the i^{th} interfering BS, respectively, while g and h_i denote the corresponding channel fading power, which are independent and identically exponentially distributed (i.i.d.) with a unit mean, i.e., $g \sim \exp(1)$ and $h_i \sim \exp(1) \forall\, i$. In MU-MIMO case, h_{ij} is the channel's fading power from the j^{th} antenna of the i^{th} interfering BS to the user and it is i.i.d. with a unit mean. Without loss of generality we have considered a user in the 0^{th} cell of Fig. 2 in our analysis.

Similar to [10], the subscribers are classified as cell-centre users and cell-edge users based on the SINR at the mobile station. If the calculated SINR of a user is lower than the specified SINR threshold S_{th}, the user is classified as a cell-edge user. Otherwise, the user is classified as a cell-centre user. Typically, FFR divides the whole frequency band into a total of $(1 + \delta)$ parts, where F_0 is allocated to all the cells for the cell-centre users, as seen in Fig. 1. One of the $\{1, \cdots, \delta\}$ parts is assigned to the cell-edge users in each cell in a planned fashion. The users are assumed to be uniformly distributed in a cell and all resource blocks are uniformly shared among the users. The transmit power is assumed to be fixed. If we have $\eta_t(r)$(or $\eta_r(r)$) $\geq S_{th}$ for a user, then the user will continue to experience the same fading power, i.e., g and h_i from the user to the serving BS and to the i^{th} interfering BS, respectively. However, if we have $\eta_t(r)$(or $\eta_r(r)$) $< S_{th}$ for a user, the user is allocated another sub-band (from the set of sub-bands assigned to cell-edge users) and it experiences a new fading power, i.e., $\hat{g}$ and $\hat{h}_i$ from the user to the serving BS and to the i^{th} interfering BS, respectively. Based on the coherence bandwidth of the OFDM system, and the bands associated with F_0 to F_3 in Fig. 1 is is possible that $\hat{g}$ and $\hat{h}_i$ are either correlated with or independent of g and h_i, respectively. Note that g, $\hat{g}$, h_i, and $\hat{h}_i$ are the channel gains in the frequency domain and the term correlation is used for referring to frequency domain correlation in this paper. The correlation depends both on the particular user's channel conditions and on the instantaneous coherence bandwidth with respect to the FFR frequency bands. To better understand the impact of correlation among the sub-bands on the FFR system's performance, in this paper, we consider the following two extreme cases:

Case 1: g and $\hat{g}$ are independent and also h_i as well as $\hat{h}_i$, are independent for all i.

Case 2: g and $\hat{g}$ are fully correlated and also h_i as well as $\hat{h}_i$, are fully correlated for all i.

In reality these channel output powers may be partially correlated, but the analysis of partial (arbitrary) correlation is quite complicated and hence it is beyond the scope of this work. However, the analysis of the above two extreme cases we believe, is sufficient for understanding the impact of correlation among the sub-bands.

III. Coverage Probability Analysis of FFR

In this section, we first derive the CP_r of both the MU-MIMO and SIMO system considered, which is defined as the probability that a randomly chosen user's instantaneous SINR $\eta_t(r)$ is higher than T. This defines, the average fraction of users are having an SINR higher than the target SINR. The coverage probability is determined by the complementry cumulative distribution function of the SINR over the network. The

[3]It is widely exploited that using the LMMSE receiver $(N_r - 1)$ interferers can be mitigated, where N_r is the number of receive antennas [32]. However, for simplicity, we assume that the $N_r - 1$ closest interferers can be completely cancelled.

[4]Typically, the path loss model is assumed to be $\max\{d, \|x\|\}^{-\alpha}$.

IEEE Proof

CP_r of a user who is at a distance of r meters from the BS in a FR1-aided MU-MIMO scenario is given by

$$P_1(T,r) = P\left[\eta_t(r) > T\right] = P\left[g > Tr^{\alpha} I_t + Tr^{\alpha}\frac{\sigma^2}{P}\right], \quad (3)$$

where I_t is defined in (2). Since $g \sim \exp(1)$, $h_{ij} \sim \exp(1)$, and h_{ij} are i.i.d., $P_1(T,r)$ is given by

$$P_1(T,r) = E_{h_{ij}}\left[e^{-Tr^{\alpha}I_t - Tr^{\alpha}\frac{\sigma^2}{P}}\right] = \prod_{i\in\psi}\prod_{j=1}^{N_t} E_{h_{ij}}\left[e^{-Tr^{\alpha}h_{ij}d_i^{-\alpha}}\right] \times e^{-Tr^{\alpha}\frac{\sigma^2}{P}} = \prod_{i\in\psi}\left(\frac{1}{1+Tr^{\alpha}d_i^{-\alpha}}\right)^{N_t} e^{-Tr^{\alpha}\frac{\sigma^2}{P}}, \quad (4)$$

where ψ is the set of interfering BSs in a FR1 network. Similarly, the CP_r of a user located at a distance of r meters from the BS in a FR3 network can be formulated as

$$P_3(T,r) = \prod_{i\in\phi}\left(\frac{1}{1+Tr^{\alpha}d_i^{-\alpha}}\right)^{N_t} e^{-Tr^{\alpha}\frac{\sigma^2}{P}} \quad (5)$$

where ϕ is the set of interfering cells in the FR3 scheme, which is a function of the frequency reuse plan. Also, the CP_r of a user in the SIMO-based FR1 network and in a FR3 network can be expressed as

$$P_1(T,r) = \prod_{i\in\psi_r}\frac{1}{1+Tr^{\alpha}d_i^{-\alpha}}e^{-Tr^{\alpha}\frac{\sigma^2}{P}} \quad \text{and}$$
$$P_3(T,r) = \prod_{i\in\phi_r}\frac{1}{1+Tr^{\alpha}d_i^{-\alpha}}e^{-Tr^{\alpha}\frac{\sigma^2}{P}}. \quad (6)$$

Here ϕ_r denotes the set of interfering cells in the FR3 scheme excluding the nearest (N_r-1) interferers. Let us now derive the CP_r of FFR for both the independent and correlated cases.

A. Case 1: g and $\hat{g}$ are Independent as Well as h_i and $\hat{h}_i$ are Also Independent for all i

The CP_r $P_{F,c}(r)$ of a cell-centre user who is at a distance of r meters from the 0^{th} BS in a FFR-aided MU-MIMO scenario is given by

$$P_{F,c}(r) \overset{(a)}{=} P\left[\eta_t(r) > T | \eta_t(r) > S_{th}\right] = P\left[\frac{gr^{-\alpha}}{I_t+\frac{\sigma^2}{P}} > T \middle| \frac{gr^{-\alpha}}{I_t+\frac{\sigma^2}{P}} > S_{th}\right],$$

where (a) follows from the fact that a cell-centre user has SINR $\geq S_{th}$. Upon applying Bayes' rule, one can rewrite $P_{F,c}(r)$ as

$$P_{F,c}(r) = \frac{P\left[\frac{gr^{-\alpha}}{I_t+\frac{\sigma^2}{P}} > T,\ \frac{gr^{-\alpha}}{I_t+\frac{\sigma^2}{P}} > S_{th}\right]}{P\left[\frac{gr^{-\alpha}}{I_t+\frac{\sigma^2}{P}} > S_{th}\right]} = \frac{\prod_{i\in\psi}\left(\frac{1}{1+\max\{T,S_{th}\}r^{\alpha}d_i^{-\alpha}}\right)^{N_t} e^{-\max\{T,S_{th}\}r^{\alpha}\frac{\sigma^2}{P}}}{\prod_{j\in\psi}\left(\frac{1}{1+S_{th}r^{\alpha}d_j^{-\alpha}}\right)^{N_t} e^{-S_{th}r^{\alpha}\frac{\sigma^2}{P}}}. \quad (7)$$

Similarly, the CP_r of a cell-edge user who is at a distance of r meters from the BS in the FFR-aided MU-MIMO case $P_{F,e}(r)$ is given by

$$P_{F,e}(r) = P\left[\hat{\eta}_t(r) > T | \eta_t(r) < S_{th}\right] = \frac{P\left[\frac{\hat{g}r^{-\alpha}}{\hat{I}_t+\frac{\sigma^2}{P}} > T,\ \frac{gr^{-\alpha}}{I_t+\frac{\sigma^2}{P}} < S_{th}\right]}{P\left[\frac{gr^{-\alpha}}{I_t+\frac{\sigma^2}{P}} < S_{th}\right]}.$$

Here, the cell-edge user will experience the new interference term of $\hat{I}_t = \sum_{i\in\phi}\sum_{j=1}^{N_t}\hat{h}_{ij}d_i^{-\alpha}$ and the new channel power $\hat{g}$, i.e. a new SINR $\hat{\eta}(r)$ due to the fact that the cell-edge user is now a FR3 user. Basically, $\hat{\eta}(r)$ denotes the SINR experienced by the user at a distance of r meters from the BS in a FR3 system and is given by

$$\hat{\eta}(r) = \frac{\hat{g}r^{-\alpha}}{\hat{I}_t+\frac{\sigma^2}{P}}, \quad \hat{I}_t = \sum_{i\in\phi}\sum_{j=1}^{N_t}\hat{h}_{ij}d_i^{-\alpha}. \quad (8)$$

Since both g and $\hat{g}$ as well as h_i and $\hat{h}_i$ are assumed to be i.i.d, $P_{F,e}(r)$ can be simplified to

$$P_{F,e}(r) = P\left[\frac{\hat{g}r^{-\alpha}}{\hat{I}_t+\frac{\sigma^2}{P}} > T\right] = P_3(T,r). \quad (9)$$

Let us now derive the CP_r $P_f(r)$ of a user in the FFR-aided MU-MIMO system, which can be written as

$$P_F(r) = P_{F,c}(r)P\left[\eta_t(r) > S_{th}\right] + P_{F,e}(r)P\left[\eta_t(r) < S_{th}\right]. \quad (10)$$

Here, the first term denotes the CP_r contributed by the cell-centre users, while the second term denotes the contribution of the cell-edge users. By using the expression in (7) for $P_{F,c}(r)$ and the expression in (9) for $P_{F,e}(r)$, (10) can be simplified to

$$P_F(r) = \prod_{i\in\psi}\left(\frac{1}{1+\max\{T,S_{th}\}r^{\alpha}d_i^{-\alpha}}\right)^{N_t} e^{-\max\{T,S_{th}\}r^{\alpha}\frac{\sigma^2}{P}} + P_3(T,r) - P_3(T,r)P_1(S_{th},r). \quad (11)$$

Lemma 1: The optimum S_{th} (denoted by $S_{opt,C}$) that maximizes the FFR-aided coverage probability is $S_{th} = T$, and when the SINR threshold is set to $S_{opt,c}$, the coverage probability of FFR becomes higher than that of FR3.

Proof: See Appendix A for the proof. □

B. Case 2: g and $\hat{g}$ are Completely Correlated as Well as h_i and $\hat{h}_i$ are Also Completely Correlated for all i

Note that the centre CP_r is the same for both the above Case 1 and for this case, since a user does not change its sub-band, when it becomes a cell-centre user because if $\eta_t(r) \geq S_{th}$ for a user, then it will continue to experience the same fading power. However, the edge CP_r is different in Case 1 as well as Case 2, and in this scenario the CP_r $P_{F,e}(r)$ of a cell-edge user,

IEEE Proof

who is at a distance of r meters from the BS in our FFR network is given by

$$P_{F,e}(r)=P\left[\hat{\eta}_t(r)>T|\eta_t(r)<S_{th}\right]=\frac{P\left[\hat{\eta}_t(r)>T,\,\eta_t(r)<S_{th}\right]}{P\left[\eta_t(r)<S_{th}\right]}. \tag{12}$$

Substituting the value of $P_{F,c}$ and $P_{F,e}$ from (7) and (12) into Eq. (10), the CP$_r$ $P_f(r)$ in our FFR network can be written as

$$P_F(r)=\prod_{i\in\psi}\left(\frac{1}{1+\max\{T,S_{th}\}r^{\alpha}d_i^{-\alpha}}\right)^{N_t}e^{-\max\{T,S_{th}\}r^{\alpha}\frac{\sigma^2}{P}} + P\left[\hat{\eta}_t(r)>T,\,\eta_t(r)<S_{th}\right]. \tag{13}$$

Recall that $\eta_t(r)$ and $\hat{\eta}_t(r)$ represent the SINR experienced by a user in an FR1 and an FR3 system, respectively. Note that even though g and $\hat{g}$ as well as h_i and $\hat{h}_i$ are completely correlated, $\eta_t(r)$ is not the same as $\hat{\eta}_t(r)$, because the set of interferers are different in the denominator of the $\eta_t(r)$ and $\hat{\eta}_t(r)$ expressions given in (2) and (8), respectively, i.e., ψ corresponds to the set of interferers in the FR1 network, while ϕ corresponds to the set of interferers in the FR3 network. Since g and $\hat{g}$ are completely correlated and h_i and $\hat{h}_i$ are also completely correlated for all i, we use the following transformation to further simplify $P_F(r)$:

$$P\left[\hat{\eta}_t(r)>T,\,\eta_t(r)<S_{th}\right]=P\left[\hat{\eta}_t(r)>T,\,\hat{\eta}_t(r)<\hat{S}_{th}\right]. \tag{14}$$

Basically instead of marking a user as a cell-edge user based on the FR1 SINR $\eta_t(r)$, we mark them on the basis of the FR3 SINR $\hat{\eta}_t(r)$ by introducing a new SINR threshold $\hat{S}_{th}$. In other words, we introduce a new SINR threshold $\hat{S}_{th}$ for ensuring that if for any user we have $\eta_t(r)<S_{th}$, then for the same user we have $\hat{\eta}_t(r)<\hat{S}_{th}$ and vice-versa. The threshold $\hat{S}_{th}$ is computed using the relationship of $P[\eta_t(r)<S_{th}]=P[\hat{\eta}_t(r)<\hat{S}_{th}]$. This ensures that the same user is marked as a cell-edge user for both reuse patterns FR1 and FR3. Now, using the transformation given in (14), $P_F(r)$ can be simplified to

$$P_F(r)=\prod_{i\in\psi}\left(\frac{1}{1+\max\{T,S_{th}\}r^{\alpha}d_i^{-\alpha}}\right)^{N_t}e^{-\max\{T,S_{th}\}r^{\alpha}\frac{\sigma^2}{P}} + P\left[\hat{\eta}(r)>T\right]-P\left[\hat{\eta}(r)>\max\{\hat{S}_{th},T\}\right]. \tag{15}$$

In this case, to obtain the optimum $S_{opt,C}$, we consider the following two possibilities: (*i*) $S_{th}\geq T$, (*ii*) $S_{th}<T$.

(i) $S_{th}\geq T$: In this scenario, $CP_f(r)$ can be expressed in terms of T as:

$$P_F(r,S_{th}\geq T)=\prod_{i\in\psi}\frac{1}{1+S_{th}r^{\alpha}d_i^{-\alpha}}e^{-S_{th}r^{\alpha}\frac{\sigma^2}{P}} + P_3(T,r)-P_3(\hat{S}_{th},r). \tag{16}$$

Since we have $P_3(\hat{S}_{th},r)=P_1(S_{th},r)$ and $P_1(S_{th},r)=\prod_{i\in\psi}\left(\frac{1}{1+S_{th}r^{\alpha}d_i^{-\alpha}}\right)^{N_t}e^{-S_{th}r^{\alpha}\frac{\sigma^2}{P}}$, hence

$$P_F(r,S_{th}\geq T)=P_3(T,r). \tag{17}$$

(ii) $S_{th}<T$: In this case $P_f(r)$ can be formulated in terms of T as:

$$P_F(r,S_{th}<T)=\prod_{i\in\psi}\left(\frac{1}{1+Tr^{\alpha}d_i^{-\alpha}}\right)^{N_t}e^{-Tr^{\alpha}\frac{\sigma^2}{P}} + P_3(T,r)-P_3\left(\max\{\hat{S}_{th},T\},r\right). \tag{18}$$

Note that when $S_{th}<T$, $\hat{S}_{th}$ may be higher or lower than T. When $\hat{S}_{th}>T$,

$$P_3\left(\max\{\hat{S}_{th},T\},r\right)=P_3(\hat{S}_{th},r)=P_1(S_{th},r)>P_1(T,r) \tag{19}$$

since $S_{th}<T$. And when $\hat{S}_{th}<T$, we have:

$$P_3\left(\max\{\hat{S}_{th},T\},r\right)=P_3(T,r)>P_1(T,r). \tag{20}$$

Hence, we arrive at:

$$P_F(r,S_{th}<T)=\prod_{i\in\psi}\left(\frac{1}{1+Tr^{\alpha}d_i^{-\alpha}}\right)^{N_t}e^{-Tr^{\alpha}\frac{\sigma^2}{P}} + P_3(T,r)-P_3\left(\max\{\hat{S}_{th},T\},r\right)<P_3(T,r). \tag{21}$$

Comparing the FFR CP$_r$ for $S_{th}\geq T$ and $S_{th}<T$ given by (17) and (21), respectively, it becomes apparent that $P_F(r,S_{th}\geq T)>P_F(r,S_{th}<T)$. In other words, when the fading is fully correlated across the sub-bands, the optimal choice of the SINR threshold is $S_{th}\geq T$ and at the optimal SINR threshold the FFR scheme succeeds in achieving the FR3 CP$_r$. Unlike for Case 1, the FFR CP$_r$ is not better than the FR3 CP$_r$ since there is no sub-band diversity gain, when a user moves from the cell-centre to the cell-edge region.

In order to find the CP$_r$ for a typical user, we have to calculate the probability density function (pdf) of r, which is the distance between the 0^{th} BS (serving BS) and the desired user. To calculate this pdf, we model the cell shape by an inner circle within a hexagonal cell [33], and assume that the users are uniformly distributed. Therefore, the pdf $f_R(r)$ of r is given by

$$f_R(r)=\begin{cases}\frac{2r}{R^2},\ r\leqslant R\\ 0,\ r>R.\end{cases} \tag{22}$$

IV. Average Rate

In this section, we derive the average rate of both the FFR-aided MU-MIMO as well as of its SIMO counterpart and find the optimum value of S_{th} (denoted by $S_{opt,R}$) for which the average rate is maximum. The average rate of the system is given by $R=E[\ln(1+\text{SINR})]$. In order to derive the average rate[5] for the FFR system, we have to consider its sub-band allocation. Since the users are uniformly distributed, the specific sub-band allocated to the cell-centre users and cell-edge users are given by [9], [10] $N_c=N_tP_{F,c}$ and $N_e=\frac{N_t-N_c}{3}$, where $P_{F,c}$ denotes the specific fraction of cell-centre users, while N_t, N_c and N_e denote the total band, cell-centre sub-band and cell-edge

[5] An interference limited system is assumed for simplicity, which implies ignoring the effects of noise. However, the derivation of the average rate can be readily extended to the case, where the thermal noise is also considered.

IEEE Proof

sub-band, respectively. Let us now derive the average rate for the planned FFR-aided MU-MIMO case.

A. Average Rate in the FR1 and FR3 Systems

The average rate of a user at a distance r is $E[\ln(1+\eta_t(r))]$. By exploiting the fact that for a positive random variable $X = \ln(1+\eta_t(r))$ we have $E[X] = \int_{t>0} P(X>t)\mathrm{d}t$, the rate $R_1(r)$ can be rewritten as

$$R_1(r) = \int\limits_{t>0} P[\ln(1+\eta_t(r)) > t]\mathrm{d}t = \int\limits_{t>0} P[\eta_t(r) > e^t - 1]\mathrm{d}t$$
$$= \int\limits_{t>0} \prod_{j\in\psi} \left(\frac{1}{1+(e^t-1)r^\alpha d_j^{-\alpha}}\right)^{N_t} \mathrm{d}t, \tag{23}$$

which follows from (3) and (4). Let us now determine the average rate of the FR1 system, where spatially averaged rate R_1 can be expressed as

$$R_1 = \int\limits_0^R \int\limits_{t>0} \prod_{j\in\psi} \left(\frac{1}{1+(e^t-1)r^\alpha d_j^{-\alpha}}\right)^{N_t} \mathrm{d}t f_R(r)\mathrm{d}r. \tag{24}$$

The average rate of FR3 can be obtained in a similar fashion, which is given by

$$R_3 = \int\limits_0^R \int\limits_{t>0} \prod_{i\in\phi} \left(\frac{1}{1+(e^t-1)r^\alpha d_i^{-\alpha}}\right)^{N_t} \mathrm{d}t f_R(r)\mathrm{d}r. \tag{25}$$

B. Average Rate of the FFR System, When the Sub-Bands are Independent

Lemma 2: The average rate of the FFR-aided MU-MIMO system is given by

$$R_f = \int\limits_0^R \int\limits_{t>0} \left(\prod_{j\in\psi} \left(\frac{1}{1+\max\{e^t-1, S_{th}\} r^\alpha d_j^{-\alpha}}\right)^{N_t} + \frac{1}{3}\prod_{i\in\phi} \frac{P[\eta_t(r) < S_{th}]}{\left(1+(e^t-1)r^\alpha d_i^{-\alpha}\right)^{N_t}}\right) \mathrm{d}t f_R(r)\mathrm{d}r. \tag{26}$$

Proof: See Appendix B for the proof. □

Similarly, the average rate of the FFR-aided SIMO system is given by

$$R_f = \int\limits_0^R \int\limits_{t>0} \left(\prod_{j\in\psi_r} \frac{1}{1+\max\{e^t-1, S_{th}\} r^\alpha d_j^{-\alpha}} + \frac{1}{3}\prod_{i\in\phi_r} \frac{P[\eta_r(r) < S_{th}]}{1+(e^t-1)r^\alpha d_i^{-\alpha}}\right) \mathrm{d}t f_R(r)\mathrm{d}r. \tag{27}$$

C. Optimum Value of the SIR Threshold $S_{opt,R}$, When the Sub-Bands are Independent

The optimum value of S_{th} (denoted by $S_{opt,R}$) for which the average rate of the FFR system is maximized is derived and it is shown to be a function of both the number of antennas and of the path loss exponent.

Lemma 3: The value of S_{th} which maximizes the average rate of the FFR system is $S_{opt,R} = T'$, where T' can be obtained as the solution of equation given in (28), shown at the bottom of the page, where, $K(r)$ is defined later in (47).

Proof: See Appendix C for the proof. □

Note that the optimal S_{th} of the SIMO scenario can be derived by following the method of the MU-MIMO case and it is $S_{opt,R} = T'$, where T' can be obtained as the solution of the equation given in (29), shown at the bottom of the page, where we have $K(r) = \frac{1}{3}\int\limits_{t>0}\prod_{i\in\phi_r} \frac{1}{1+(e^t-1)r^\alpha d_i^{-\alpha}}\mathrm{d}t$.

Fig. 3 plots the optimal SINR threshold S_{th} versus the number of antennas for different path loss exponent. It can be observed for the MU-MIMO case that as the number of transmit antennas is reduced, $S_{opt,R}$ increases. Intuitively, as the number of transmit antennas decreases, the interference experienced by the user would decrease as the interference from the other cell decrease. Thus, the average SINR of all users increases. Hence, the optimal SINR threshold increases in order to balance the ratio of cell-edge users and cell-centre users. Similarly, as the number of receive antennas increases, the average SINR increases in SIMO scenario, because more antennas are capable of cancelling more of the closest interferers. Hence, $S_{opt,R}$ increases

$$\int\limits_0^R \left(\frac{\left(K(r) - \ln(1+T')\right)\sum_{i\in\psi}\left(1+T' r^\alpha d_i^{-\alpha}\right)^{N_t-1} r^\alpha d_i^{-\alpha}\left(\prod_{j\in\psi\setminus i}\left(1+T' r^\alpha d_j^{-\alpha}\right)^{N_t}\right)}{\left(\prod_{j\in\psi}\left(1+T' r^\alpha d_j^{-\alpha}\right)\right)^{2N_t}}\right) f_R(r)\mathrm{d}r = 0, \tag{28}$$

$$\int\limits_0^R \left(\frac{\left(K(r) - \ln(1+T')\right)\sum_{i\in\psi_r} r^\alpha d_i^{-\alpha}\left(\prod_{j\in\psi_r\setminus i}\left(1+T' r^\alpha d_j^{-\alpha}\right)\right)}{\left(\prod_{j\in\psi_r}\left(1+T' r^\alpha d_j^{-\alpha}\right)\right)^{2}}\right) f_R(r)\mathrm{d}r = 0, \tag{29}$$

IEEE Proof

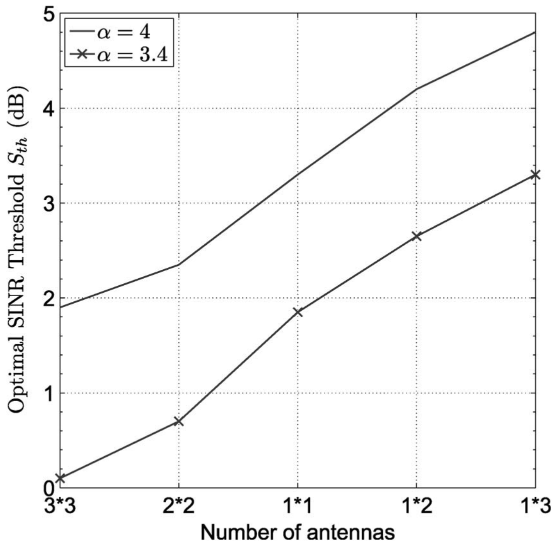

Fig. 3. Optimal SINR threshold S_{th} evaluated using (28) and (29) versus the number of antennas for different path-loss exponents.

in order to balance the ratio of cell-centre users and cell-edge users. Furthermore, as the path loss exponent decreases, the average SIR of all the users decreases and hence $S_{opt,R}$ decreases.

D. Average Rate of the FFR System, When the Sub-Bands are Completely Correlated

In this subsection first we derive the average rate $R_f(r)$ of the FFR system for the MU-MIMO case. The average rate of the FFR system given in (39) can be rewritten as

$$R_f(r) = R_c(r)P\left[\eta_t(r) > S_{th}\right] + \frac{1}{3}R_e(r)P\left[\eta_t(r) < S_{th}\right]. \quad (30)$$

Note that the first term $R_c(r)P[\eta_t(r) > S_{th}]$ denotes the average rate contributed by the cell-centre users and it is the same regardless, whether the fading of the bands is correlated or independent across the sub-bands. Similar to the average rate of the FFR system given in (39), the factor $\frac{1}{3}$ is introduced in the second term, since a frequency reuse factor of $\frac{1}{3}$ is invoked for the cell-edge users. In other words, only one third of the cell-edge frequency $(F_1 + F_2 + F_3)$ is used for the cell-edge users and hence the factor $\frac{1}{3}$ multiplies the second term of (30). Now, using the expression of $R_e(r)$ in (42), $R_e(r)P[\eta_t(r) < S_{th}]$ can be written as

$$R_e(r)P\left[\eta_t(r) < S_{th}\right] = \int\limits_{t>0} P\left[\hat{\eta}_t(r) > e^t - 1,\, \eta_t(r) < S_{th}\right] \mathrm{d}t. \quad (31)$$

Using the transformation in (14), $R_e(r)P[\eta_t(r) < S_{th}]$ can be simplified to

$$R_e(r)P\left[\eta_t(r) < S_{th}\right] = \int\limits_{t>0} P\left[\hat{\eta}_t(r) > e^t - 1\right] - P\left[\hat{\eta}_t(r) > \max\{e^t - 1, \hat{S}_{th}\}\right] \mathrm{d}t. \quad (32)$$

Using the result of (25), $R_e(r)P[\eta(r) < S_{th}]$ can be further simplified to

$$R_e(r)P\left[\eta_t(r) < S_{th}\right] = \int\limits_{t>0} \prod_{i\in\phi} \frac{1}{1 + (e^t - 1)r^{\alpha} d_i^{-\alpha}} - \prod_{i\in\phi} \frac{1}{1 + \max\{e^t - 1, \hat{S}_{th}\}r^{\alpha} d_i^{-\alpha}} \mathrm{d}t. \quad (33)$$

Finally, substituting back (41) as well as (33) into (30) and then averaging over the spatial dimension, the average rate of the FFR system is given as

$$R_f = \int_0^R \int\limits_{t>0} \prod_{j\in\psi} \frac{1}{1+\max\{e^t-1, S_{th}\}r^{\alpha} d_j^{-\alpha}} + \frac{1}{3}\left(\prod_{i\in\phi} \frac{1}{1+(e^t-1)r^{\alpha} d_i^{-\alpha}} - \prod_{i\in\phi} \frac{1}{1+\max\{e^t-1, \hat{S}_{th}\}r^{\alpha} d_i^{-\alpha}}\right) \mathrm{d}t f_R(r)\mathrm{d}r. \quad (34)$$

V. Simulation Results

In this section, we provide the simulation results in order to verify our analytical results In the simulations, we have considered the classic 19 cell system associated with a hexagonal structure having a radius of 1000 meters. A LTE system having a 10 MHz bandwidth, 50 physical resource blocks (PRB) and 25 users is considered for each cell. The users are assumed to be uniformly distributed in a cell and similarly, all resource blocks are uniformly shared among users. In other words, if there are K users and R resource blocks then each user is assigned $\frac{R}{K}$ resource blocks. For each user we generate the channel fading power corresponding to its own channel as well as that corresponding to the 18 interferers and then compute the SIR per user per PRB. If a user having an SIR higher than S_{th} over 25 or more than 25 PRBs, then the user is considered to be a cell-centre user, otherwise it is classified as a cell-edge user. For the analytical CP_r computation, (11) and (15) are used for the independent and correlated cases, respectively. Fig. 4 shows the variation of CP_r as a function of the SINR threshold for FR1, FR3, and the FFR case using both our analytical expressions in (11) and (15) and simulations. Observe in Fig. 4 that the analytical results match the simulation results. It can be seen that for the independent fading case, the CP_r reaches its maximum, when $S_{th} = T$ and it becomes higher than the FR3 CP_r. However, for the fully correlated case, the CP_r becomes maximum, when $S_{th} \geq T$ and it is equal to the FR3 CP_r.

Note that all our results are based on considering Rayleigh fading. However, the results seem to be valid for general fading. For example, Fig. 5 shows the variation of CP_r as a function of the SINR threshold by considering Nakagami-m fading using simulations. The CP_r is shown for the FR1, FR3 and FFR scenarios for the different values of the Nakagami shape parameter m. Similar to the Rayleigh fading scenario, the CP_r reaches its maximum, when $S_{th} = T$ and it becomes higher than the FR3 CP_r. Interestingly, as the Nakagami shape parameter increases, the gap between the optimal FFR CP_r and FR3 CP_r

IEEE Proof

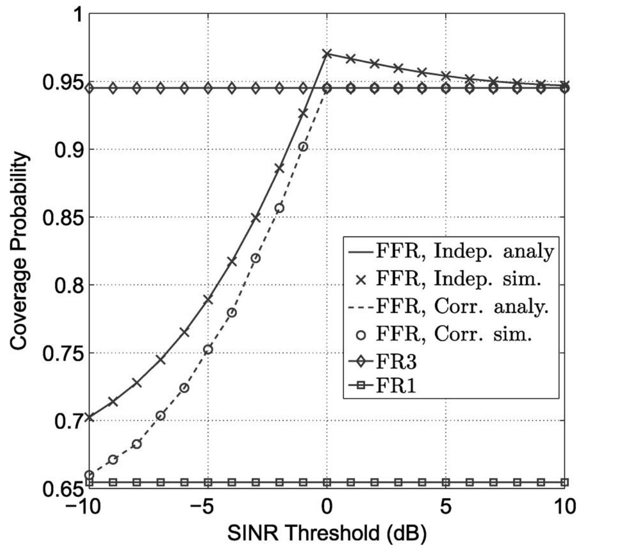

Fig. 4. Coverage probability of FR1, FR3 and FFR evaluated for (11) and (15) with respect to SINR Threshold S_{th}. Here, $T = 0$ dB, $\alpha = 3.2$ and $N_t = N_r = 1$.

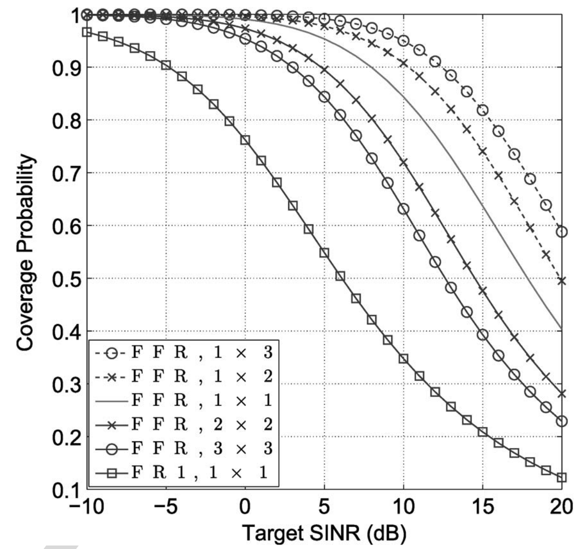

Fig. 6. Coverage probability of both FR1 and of FFR-aided MU-MIMO and SIMO case evaluated for (11) versus the target SINR T. Here we have $\alpha = 4$ and $S_{th} = T$ dB, $\delta = 3$.

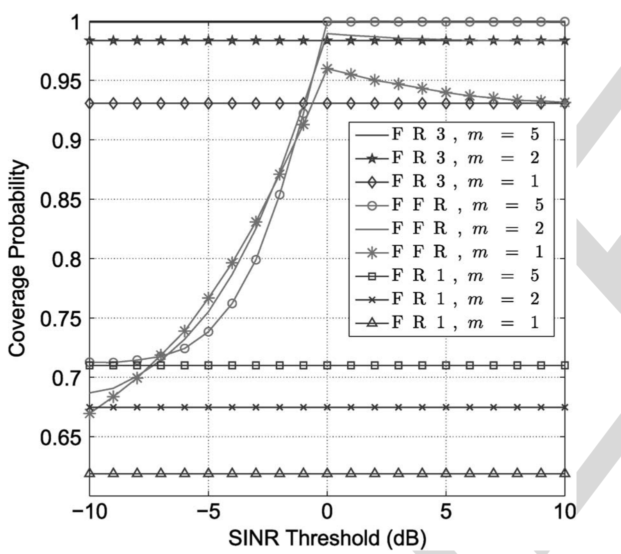

Fig. 5. Coverage probability of FR1, FR3 and FFR for different value of shape parameter for Nakagami-m fading. Here, $T = 0$ dB, $\alpha = 3$ and $N_t = N_r = 1$.

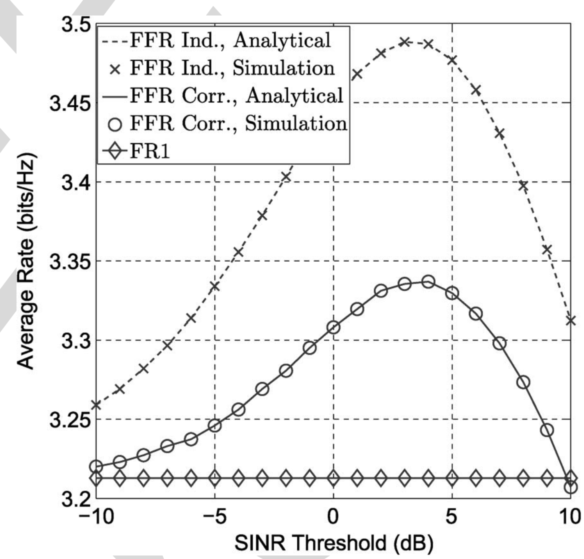

Fig. 7. Average rate of FR1 and FFR versus the SINR threshold. Here we have $\alpha = 4$, $N_t = N_r = 1$. The theoretical results are plotted from Eq. (26) and (34).

decreases and it almost becomes negligible, when the shape parameter is in excess of $m = 5$.

Fig. 6 depicts the CP_r of the FFR-aided MU-MIMO and SIMO systems at the optimal value of S_{th} with respect to the target SINR. The CP_r of FR1 is also plotted for reference. It can be observed in Fig. 6 that the FR1 CP_r is significantly lower than that of FFR-aided MU-MIMO. The CP_r of the FFR-aided SIMO case is higher than that of the FFR-aided MU-MIMO scenario.

Fig. 7 plots the average rate of both the FFR and FR1 systems versus the SINR threshold. For plotting the analytical result, (26) and (34) are used for the independent and correlated case, respectively. Observe that the simulation results closely match the analytical results. Firstly, it can be seen that the FFR achieves the maximum value of the average rate at 3.3 dB, which is the $S_{opt,R}$ value, as shown in Fig. 3 for a (1×1)-antenna system. Secondly, it can be observed in Fig. 7 that the average rate is reduced, when the sub-bands are correlated. Furthermore, interestingly, the optimal SINR threshold of the correlated case is nearly the same as the optimal SINR threshold of the independent fading case. Although, we have considered continuous log-shaped curve mapping between the SINR and the data rate, in practical scenarios, the mapping is given by discrete curves asscociated with different modulation and coding schemes (MCSs). Therefore, we have also provided the average rate versus the SINR threshold based on the specific MCS level using simulation results as shown in Fig. 8. The mapping between SINR and data rate is based on Table 10.1 of the [34]. It can be observed that the value of $S_{opt,R}$ is the same as observed in Fig. 7. Furthermore, the optimal SINR threshold of the correlated case is nearly the same as the optimal SINR threshold of the independent fading scenario.

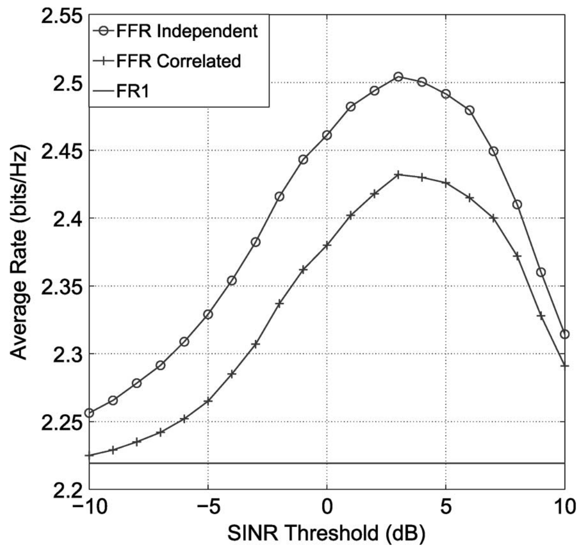

Fig. 8. Average rate of FR1 and FFR using MCS labels versus the SINR threshold. Here we have $\alpha = 4$, $N_t = N_r = 1$.

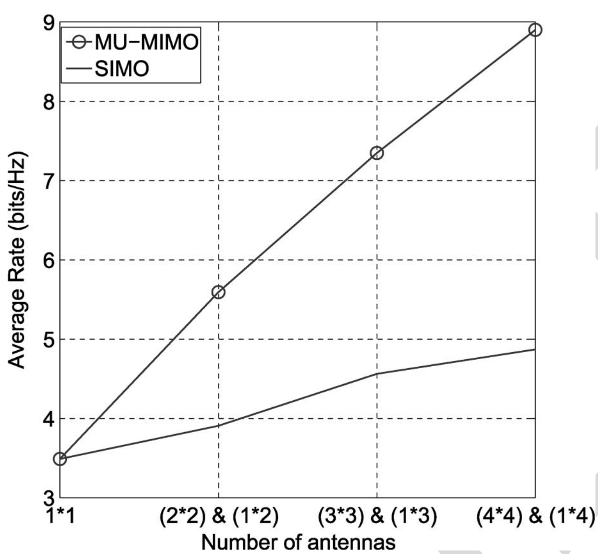

Fig. 9. Maximum average rate achieved by the FFR-aided MU-MIMO and SIMO systems evaluated using (26) and (27) versus the number of antennas for $\alpha = 4$.

Let us now compare the average rate achieved by the MU-MIMO and SIMO scenarios at the optimal SINR thresholds. Fig. 9 plots the average rate achieved by the MU-MIMO and SIMO scenarios versus the number of antennas. It is interesting to note that the average rate achieved by the MU-MIMO case is significantly higher than that of the SIMO case. For example, the average rate achieved by the (2×2) MU-MIMO case and by the (1×3) SIMO case are 5.6 bits/Hz and 4.56 bits/Hz, respectively. In other words, the (2×2) MU-MIMO system achieves a 22.5% higher rate than the (1×3) SIMO system. However, the overall CP_r achieved by the SIMO case is higher than that of the MU-MIMO case. Now a natural question arises, which of the systems should be chosen by the system designer, since both the CP_r as well as the average rate are important metrics. Based on our results, system designer may opt for the (2×2) MU-MIMO system over the (1×3) SIMO system, since the gain in average rate is significant and the CP_r degradation for (2×2) MU-MIMO is low for lower target SINRs.

Finally, we have two different expressions for optimal SINR threshold for both the cases, one corresponding to CP_r $(S_{th} = T)$ and other corresponding to average rate $(S_{th} = T')$. To maximize both CP_r as well as average rate simultaneously, the system designer would have to choose one of these two expressions. Now the question arises as to which expression is more appropriate? In order to answer this, we first discuss the benefit of FFR. We see from Figs. 3 and 4 that FFR provides 48% gain in CP_r and 8.5% gain in average rate with respect to FR1 at the optimal S_{th}. In other words, FFR provides significantly high gain in CP_r and hence this scheme would be more useful when coverage gain is essentially required. Therefore, FFR-aided MU-MIMO provides both high average rate and satisfactory CP_r, since due to MU-MIMO average rate is high and due to FFR scheme CP_r is satisfactory. It can be also noted from Fig. 4 that when S_{th} is higher than the optimal S_{th}, the loss in CP_r is negligible, while when S_{th} is lower than the optimal S_{th}, there is significant change in CP_r. Hence, for the lower target SINR scenario, i.e., $T < T'$, the system designer should choose optimal S_{th} corresponding to average rate $(S_{th} = T')$. On the other hand, for higher target SINR scenario, i.e., $T > T'$, the system designer should choose optimal S_{th} corresponding to CP_r $(S_{th} = T)$.

VI. Conclusion

We have derived expressions for both the CP_r and average rate of MU-MIMO and SIMO systems based on a planned FFR deployment. The impact of frequency-domain correlation between the sub-bands allocated to the FR1 and FR3 regions on the average rate and on the CP_r was analysed in detail, since any practical OFDMA system will typically experience frequency-domain correlation. We analytically determined the optimal SINR threshold, which maximizes the CP_r, and also determined the optimal SINR threshold (denoted by $S_{opt,R}$), which maximizes the average rate for both the MU-MIMO and SIMO systems considered. It was shown that for the optimal choice of the SINR threshold, the CP_r of the FFR system is higher than that of its FR3 counterpart. The value of $S_{opt,R}$ increases, when the number of antennas is reduced in a MU-MIMO, where it is assumed that the number of transmit antennas is equal to the number of receive antennas, i.e., $N_t = N_r = N_a$. However, it increases when the number of receive antennas increases in the SIMO scenario. Furthermore, the performance of FFR of the MU-MIMO system and SIMO system are compared. It was shown that $(N_a \times N_a)$-element FFR-aided MU-MIMO achieves a significantly higher average rate than $(1 \times 2N_a - 1)$-element SIMO counterpart, but MU-MIMO achieves a lower coverage quality than its SIMO counterpart. However its average rate improvement is more significant than its CP_r reduction, especially for a lower value of N_a and for a lower target SINR. Hence a (2×2) system is preferred over a (1×3) system.

A natural extension of this work is to study the FFR-aided MU-MIMO and SIMO system in the context of the cellular uplink [35], [36]. In this study, we have assumed having a fixed transmission power and that the resource blocks are equitably shared by the users. Our future work could consider unequal transmit powers and the unequal allocation of the resource blocks as well as the study of both FFR-aided MU-MIMO and SIMO systems. Moreover, although strict FFR was considered in the paper, it would also be of substantial interest to study dynamic FFR-aided MU-MIMO and SIMO systems.

Appendix A

To obtain the $S_{opt,C}$, we consider the following three possibilities: (*i*) $S_{th} < T$, (*ii*) $S_{th} = T$, (*iii*) $S_{th} > T$.

(i) $S_{th} < T$: Let $S_{th} = T - \Delta$, where $\Delta > 0$, then $P_f(r)$ can be expressed as in terms of T

$$P_F(r, S_{th} < T) = \prod_{i\in\psi}\left(\frac{1}{1+Tr^{\alpha}d_i^{-\alpha}}\right)^{N_t} e^{-Tr^{\alpha}\frac{\sigma^2}{P}} + P_3(T,r) - P_3(T,r)P_1(T-\Delta,r). \quad (35)$$

(ii) $S_{th} = T$: In this case $P_f(r)$ in terms of T can be formulated as

$$P_F(r, S_{th} = T) = \prod_{i\in\psi}\left(\frac{1}{1+Tr^{\alpha}d_i^{-\alpha}}\right)^{N_t} e^{-Tr^{\alpha}\frac{\sigma^2}{P}} + P_3(T,r) - P_3(T,r)P_1(T,r). \quad (36)$$
$$= P_1(T,r)\,(1-P_3(T,r)) + P_3(T,r). \quad (37)$$

(iii) $S_{th} > T$: Let $S_{th} = T + \Delta$, where $\Delta > 0$, then $P_f(r)$ in terms of T is given by

$$P_F(r, S_{th} > T) = \prod_{i\in\psi}\left(\frac{1}{1+(T+\Delta)r^{\alpha}d_i^{-\alpha}}\right)^{N_t} e^{-(T+\Delta)r^{\alpha}\frac{\sigma^2}{P}} + P_3(T,r) - P_3(T,r)P_1(T+\Delta,r).$$
$$= P_1(T+\Delta,r)\,(1-P_3(T,r)) + P_3(T,r). \quad (38)$$

Let us now compare the FFR CP_r for $S_{th} < T$ and $S_{th} = T$ given by (35) and (36), respectively. Since we have $P_1(T-\Delta, r) > P_1(T,r)$, this implies that $P_F(r, S_{th} < T) < P_F(r, S_{th} = T)$. Similarly, we compare the FFR-aided CP_r for $S_{th} = T$ and $S_{th} > T$ given by (37) and (38), respectively. Since $P_1(T+\Delta, r) < P_1(T,r)$, this implies that $P_F(r, S_{th} = T) > P_F(r, S_{th} > T)$. Thus, FFR achieves the maximum achievable CP_r when $S_{th} = T$. Note that when one chooses the SINR threshold to be $S_{opt,C}$, then the CP_r of FFR is higher than that of FR3 since we have $CP_F(r, S_{th} = T) = P_1(T,r)(1-P_3(T,r)) + P_3(T,r) > P_3(T,r)$. The reason for this behaviour is as follows: only users having a low SINR (low fading gain for the desired signal and/or high fading gain for the interfering signal) move to the cell-edge region and they experience a new independent fading gain at the cell-edge region. In other words, the increase in FFR CP_r over the FR3 CP_r is due to the sub-band diversity gains which is achieved by the system, when the users move from the cell-centre to the cell-edge.

Appendix B

Since a cell-centre user is associated with $\eta_t(r) > S_{th}$, the average rate $R_c(r)$ of the cell-centre users of the FFR system can be written as $R_c(r) = E[\ln(1+\eta_t(r))|\eta_t(r) > S_{th}]$ Similarly, since a cell-edge user has $\eta_t(r) < S_{th}$, the average rate $R_e(r)$ of the cell-edge users in the FFR system can be written as $R_e(r) = E[\ln(1+\hat{\eta}_t(r))|\eta_t(r) < S_{th}]$. Now, the average rate $R_f(r)$ of the FFR system can be written as

$$R_f(r) = R_c(r)P\left[\eta_t(r) > S_{th}\right] + \frac{1}{3}R_e(r)P\left[\eta_t(r) < S_{th}\right]. \quad (39)$$

Here the first term denotes the average rate contributed by the cell-centre users, while the second term denotes the contribution of the cell-edge users. Recall that the frequency reuse $\frac{1}{3}$ is invoked for the cell-edge users. In other words, only one third of the cell-edge frequency $(F_1 + F_2 + F_3)$ is used for the cell-edge users and hence the factor $\frac{1}{3}$ is multiplied in the above expression. Using the methods outlined in Section IV-A, $R_c(r)P[\eta(r) > S_{th}]$ can be written as

$$R_c(r)P\left[\eta_t(r) > S_{th}\right] = \int_{t>0} P\left[\ln(1+\eta_t(r)) > t,\, \eta_t)r) > S_{th}\right]\mathrm{d}t$$
$$= \int_{t>0} P\left[\eta_t(r) > \max\{e^t - 1, S_{th}\}\right]\mathrm{d}t. \quad (40)$$

Using (3) and (4), this can be further simplified to

$$R_c(r)P\left[\eta_t(r) > S_{th}\right] = \int_{t>0}\prod_{j\in\psi}\left(\frac{1}{1+\max\{e^t-1, S_{th}\}r^{\alpha}d_j^{-\alpha}}\right)^{N_t}\mathrm{d}t. \quad (41)$$

Again, similar to Section IV-A, we can write $R_e(r)$ as

$$R_e(r) = \int_{t>0}\frac{P\left[\ln\left(1+\hat{\eta}_t(r)\right) > t,\, \eta_t(r) < S_{th}\right]}{P\left[\eta_t(r) < S_{th}\right]}\mathrm{d}t$$
$$= \int_{t>0}\frac{P\left[\hat{\eta}_t(r) > (e^t - 1),\, \eta_t(r) < S_{th}\right]}{P\left[\eta_t(r) < S_{th}\right]}\mathrm{d}t. \quad (42)$$

Since g and $\hat{g}$ are i.i.d as well as h_i and $\hat{h}_i$ are also i.i.d, hence $R_e(r)$ can be written as

$$R_e(r) = \int_{t>0}\prod_{i\in\phi}\left(\frac{1}{1+(e^t-1)r^{\alpha}d_i^{-\alpha}}\right)^{N_t}\mathrm{d}t. \quad (43)$$

Finally substituting back (41) and (43) into (39) and after averaging over the spatial dimension, the average rate of the FFR system is given by

$$R_f = \int_0^R\int_{t>0}\left(\prod_{j\in\psi}\left(\frac{1}{1+\max\{e^t-1, S_{th}\}r^{\alpha}d_j^{-\alpha}}\right)^{N_t} + \frac{1}{3}\prod_{i\in\phi}\frac{P\left[\eta_t(r) < S_{th}\right]}{\left(1+(e^t-1)r^{\alpha}d_i^{-\alpha}\right)^{N_t}}\right)\mathrm{d}t f_R(r)\mathrm{d}r. \quad (44)$$

IEEE Proof

APPENDIX C

The average rate expression can be written as

$$R_f = \int_0^R \int_{t>0} \left(\prod_{j\in\psi} \left(\frac{1}{1+\max\{e^t-1, S_{th}\} r^\alpha d_j^{-\alpha}} \right)^{N_t} + \frac{1}{3} \prod_{i\in\phi} \frac{P[\eta_t(r) < S_{th}]}{\left(1+(e^t-1) r^\alpha d_i^{-\alpha}\right)^{N_t}} \right) \mathrm{d}t f_R(r) \mathrm{d}r. \quad (45)$$

To maximize the rate R_f, we have to differentiate R_f with respect to S_{th}. In order to do that we split the first part of the integrand of R_f as given in (46), shown at the bottom of the page. Upon substituting $P[\eta_t(r) < S_{th}] = 1 - \prod_{j\in\psi} \left(\frac{1}{1+S_{th} r^\alpha d_j^{-\alpha}} \right)^{N_t}$ into Eq. (45), R_f can be rewritten as given in (47), shown at the bottom of the page. Using Leibniz's rule,[6] while differentiating R_f with respect to S_{th}, we obtain (48), shown at the bottom of the page. Simplifying $\frac{dR_f}{dS_{th}}$ and equating it to zero, one obtains $\frac{dR_f}{dS_{th}}$ as given in (48). The solution of the integral given in (48) gives the optimal S_{th}, namely $S_{opt,R}$, but obtaining $S_{opt,R}$ in a closed form is a challenging problem, as the distances d_is are also a function of r. Hence, we find the value of $S_{opt,R}$ by solving (48) numerically (using Mathematica (or Matlab)). Note that the optimal value of S_{th} is calculated at the time of network planning with the aid of Mathematica (or Matlab) to obtain the numerical values off line. We have investigated $S_{opt,R}$ as a function of the path loss exponent, of the number of transmit antennas, etc.

[6] Leibniz's rule states that if $f(x,\theta)$ is a function such that $\frac{d}{d\theta} f(x,\theta)$ exist, and it is continuous, then we have $\frac{d}{d\theta}\left(\int_{a(\theta)}^{b(\theta)} f(x,\theta)\, dx\right) = \int_{a(\theta)}^{b(\theta)} \frac{d}{d\theta}(f(x,\theta))\, dx + f(b(\theta),\theta) \frac{d}{d\theta} b(\theta) - f(a(\theta),\theta) \frac{d}{d\theta} a(\theta)$.

$$\int_{t>0} \prod_{j\in\psi} \left(\frac{1}{1+\max\{e^t-1, S_{th}\} r^\alpha d_j^{-\alpha}} \right)^{N_t} \mathrm{d}t = \int_{t>0}^{\ln(1+S_{th})} \prod_{j\in\psi} \left(\frac{1}{1+S_{th} r^\alpha d_j^{-\alpha}} \right)^{N_t} \mathrm{d}t + \int_{\ln(1+S_{th})}^{\infty} \prod_{j\in\psi} \left(\frac{1}{1+(e^t-1) r^\alpha d_j^{-\alpha}} \right)^{N_t} \mathrm{d}t \quad (46)$$

$$R_f = \int_0^R \left(\prod_{j\in\psi} \frac{\ln(1+S_{th})}{\left(1+S_{th} r^\alpha d_j^{-\alpha}\right)^{N_t}} + \int_{\ln(1+S_{th})}^{\infty} \prod_{j\in\psi} \left(\frac{1}{1+(e^t-1) r^\alpha d_j^{-\alpha}} \right)^{N_t} \mathrm{d}t + \left(1 - \prod_{j\in\psi} \left(\frac{1}{1+S_{th} r^\alpha d_j^{-\alpha}} \right)^{N_t} \right) \underbrace{\frac{1}{3} \int_{t>0} \prod_{i\in\phi} \left(\frac{1}{1+(e^t-1) r^\alpha d_i^{-\alpha}} \right)^{N_t} \mathrm{d}t}_{K(r)} \right) f_R(r) \mathrm{d}r. \quad (47)$$

$$\frac{dR_f}{dS_{th}} = \int_0^R \left(\frac{ \frac{\prod_{j\in\psi} \left(1+S_{th} r^\alpha d_j^{-\alpha}\right)^{N_t}}{1+S_{th}} - \ln(1+S_{th}) \frac{d}{dS_{th}} \left(\prod_{j\in\psi} \left(1+S_{th} r^\alpha d_j^{-\alpha}\right)^{N_t} \right) }{ \left(\prod_{j\in\psi} \left(1+S_{th} r^\alpha d_j^{-\alpha}\right) \right)^{2N_t} } - \prod_{j\in\psi} \frac{1}{\left(1+S_{th} r^\alpha d_j^{-\alpha}\right)^{N_t}} \left(\frac{1}{1+S_{th}} \right) + \frac{ K(r) \frac{d}{dS_{th}} \left(\prod_{j\in\psi} \left(1+S_{th} r^\alpha d_j^{-\alpha}\right)^{N_t} \right) }{ \left(\prod_{j\in\psi} \left(1+S_{th} r^\alpha d_j^{-\alpha}\right) \right)^{2N_t} } \right) f_R(r) \mathrm{d}r.$$

$$\frac{dR_f}{dS_{th}} = \int_0^R \left(\frac{ \left(K(r) - \ln(1+S_{th})\right) \sum_{i\in\psi} \left(1+S_{th} r^\alpha d_i^{-\alpha}\right)^{N_t-1} r^\alpha d_i^{-\alpha} \left(\prod_{j\in\psi\setminus i} \left(1+S_{th} r^\alpha d_j^{-\alpha}\right)^{N_t} \right) }{ \left(\prod_{j\in\psi} \left(1+S_{th} r^\alpha d_j^{-\alpha}\right) \right)^{2N_t} } \right) f_R(r) \mathrm{d}r = 0 \quad (48)$$

IEEE Proof

References

[1] G. Boudreau *et al.*, "Interference coordination and cancellation for 4G networks," *IEEE Commun. Mag.*, vol. 47, no. 4, pp. 74–81, Apr. 2009.

[2] N. Himayat, S. Talwar, A. Rao, and R. Soni, "Interference management for 4G cellular standards [WIMAX/LTE UPDATE]," *IEEE Commun. Mag.*, vol. 48, no. 8, pp. 86–92, Aug. 2010.

[3] F. Wang *et al.*, "Mobile WiMAX systems: Performance and evolution," *IEEE Commun. Mag.*, vol. 46, no. 10, pp. 41–49, Oct. 2008.

[4] D. Astely *et al.*, "LTE: The evolution of mobile broadband," *IEEE Commun. Mag.*, vol. 47, no. 4, pp. 44–51, Apr. 2009.

[5] A. S. Hamza, S. S. Khalifa, H. S. Hamza, and K. Elsayed, "A survey on inter-cell interference coordination techniques in OFDMA-based cellular networks," *IEEE Commun. Surveys Tuts.*, vol. 15, no. 4, pp. 1642–1670, 4th Quart. 2013.

[6] R. Y. Chang, Z. Tao, J. Zhang, and C.-C. J. Kuo, "A graph approach to dynamic Fractional Frequency Reuse (FFR) in multi-cell OFDMA networks," in *Proc. IEEE ICC*, Jun. 2009, pp. 1–6.

[7] M. Assaad, "Optimal Fractional Frequency Reuse (FFR) in multicellular OFDMA system," in *Proc. IEEE 68th VTC-Fall*, Sep. 2008, pp. 1–5.

[8] Z. Xu, G. Ye Li, C. Yang, and X. Zhu, "Throughput and optimal threshold for FFR schemes in OFDMA cellular networks," *IEEE Trans. Wireless Commun.*, vol. 11, no. 8, pp. 2776–2785, Aug. 2012.

[9] T. Novlan, J. G. Andrews, I. Sohn, R. K. Ganti, and A. Ghosh, "Comparison of fractional frequency reuse approaches in the OFDMA cellular downlink," in *Proc. IEEE Global Telecommun. Conf.*, 2010, pp. 1–5.

[10] T. D. Novlan, R. K. Ganti, A. Ghosh, and J. G. Andrews, "Analytical evaluation of fractional frequency reuse for OFDMA cellular networks," *IEEE Trans. Wireless Commun.*, vol. 10, no. 12, pp. 4294–4305, Dec. 2011.

[11] H. Zhuang and T. Ohtsuki, "A model based on Poisson point process for analyzing MIMO heterogeneous networks utilizing fractional frequency reuse," *IEEE Trans. Wireless Commun.*, vol. 13, no. 12, pp. 6839–6850, Dec. 2014.

[12] A. Mahmud and K. A. Hamdi, "A unified framework for the analysis of fractional frequency reuse techniques," *IEEE Trans. Commun.*, vol. 62, no. 10, pp. 3692–3705, Oct. 2014.

[13] D. G. Gonzalez, M. Garcia-Lozano, S. Ruiz Boque, and D. S. Lee, "Optimization of soft frequency reuse for irregular LTE macrocellular networks," *IEEE Trans. Wireless Commun.*, vol. 12, no. 5, pp. 2410–2423, May 2013.

[14] X. Tao, F. Xu, W. ur Rehman, Y. Xu, and X. Li, "A generic mathematical model based on fuzzy set theory for frequency reuse in cellular networks," *IEEE J. Sel. Areas Commun.*, vol. 31, no. 5, pp. 861–869, May 2013.

[15] L.-C. Wang and C.-J. Yeh, "3-cell network MIMO architectures with sectorization and fractional frequency reuse," *IEEE J. Sel. Areas Commun.*, vol. 29, no. 6, pp. 1185–1199, Jun. 2011.

[16] S. Kumar and S. Kalyani, "Impact of correlated interferers on coverage and rate of FFR and SFR schemes," *IEEE Trans. Veh. Technol.*, to be published. AQ3

[17] H. Chang and I. Rubin, "Optimal downlink and uplink fractional frequency reuse in cellular wireless networks" *IEEE Trans. Veh. Technol.*, to be published. AQ4

[18] O. Aliu, M. Mehta, M. Imran, A. Karandikar, and B. Evans, "A new cellular-automata-based fractional frequency reuse scheme," *IEEE Trans. Veh. Technol.*, vol. 64, no. 4, pp. 1535–1547, Apr. 2015.

[19] Q. Li, R. Hu, Y. Xu, and Y. Qian, "Optimal fractional frequency reuse and power control in the heterogeneous wireless networks," *IEEE Trans. Wireless Commun.*, vol. 12, no. 6, pp. 2658–2668, Jun. 2013.

[20] J. Zhang, R. Zhang, G. Li, and L. Hanzo, "Distributed antenna systems in fractional-frequency-reuse-aided cellular networks," *IEEE Trans. Veh. Technol.*, vol. 62, no. 3, pp. 1340–1349, Mar. 2013.

[21] S. Kumar, S. Kalyani, and K. Giridhar, "Spectrum allocation for ICIC based picocell," *IEEE Trans. Veh. Technol.*, to be published. AQ5

[22] F. Jin, R. Zhang, and L. Hanzo, "Fractional frequency reuse aided twin-layer femtocell networks: Analysis, design and optimization," *IEEE Trans. Commun.*, vol. 61, no. 5, pp. 2074–2085, May 2013.

[23] W. S. Jeon, J. Kim, and D. G. Jeong, "Downlink radio resource partitioning with fractional frequency reuse in femtocell networks," *IEEE Trans. Veh. Technol.*, vol. 63, no. 1, pp. 308–321, Jan. 2014.

[24] F. Wang and W. Wang, "Analytical evaluation of femtocell deployment in cellular networks using fractional frequency reuse," *IET Commun.*, vol. 8, no. 9, pp. 1599–1608, Jun. 2014.

[25] N. Saquib, E. Hossain, and D. I. Kim, "Fractional frequency reuse for interference management in lte-advanced hetnets," *IEEE Wireless Commun.*, vol. 20, no. 2, pp. 113–122, Apr. 2013.

[26] J. Y. Lee, S. J. Bae, Y. M. Kwon, and M. Y. Chung, "Interference analysis for femtocell deployment in OFDMA systems based on fractional frequency reuse," *IEEE Commun. Lett.*, vol. 15, no. 4, pp. 425–427, Apr. 2011.

[27] Q. H. Spencer, A. L. Swindlehurst, and M. Haardt, "Zero-forcing methods for downlink spatial multiplexing in multiuser MIMO channels," *IEEE Trans. Signal Process.*, vol. 52, no. 2, pp. 461–471, Feb. 2004.

[28] D. Gesbert, M. Kountouris, R. W. Heath, C.-B. Chae, and T. Salzer, "Shifting the MIMO paradigm," *IEEE Signal Process. Mag.*, vol. 24, no. 5, pp. 36–46, Sep. 2007.

[29] S. Jafar and A. Goldsmith, "Isotropic fading vector broadcast channels: The scalar upper bound and loss in degrees of freedom," *IEEE Trans. Inf. Theory*, vol. 51, no. 3, pp. 848–857, Mar. 2005.

[30] S. Catreux, P. Driessen, and L. Greenstein, "Simulation results for an interference-limited multiple-input multiple-output cellular system," *IEEE Commun. Lett.*, vol. 4, no. 11, pp. 334–336, Nov. 2000.

[31] J. G. Andrews, W. Choi, and R. W. Heath, "Overcoming interference in spatial multiplexing MIMO cellular networks," *IEEE Wireless Commun.*, vol. 14, no. 6, pp. 95–104, Dec. 2007.

[32] D. Tse and P. Viswanath, *Fundamentals of Wireless Communication*. Cambridge, U.K.: Cambridge Univ. Press, 2005.

[33] K. B. Baltzis, "Hexagonal vs circular cell shape: A comparative analysis and evaluation of the two popular modeling approximations," in *Cellular Networks-Positioning, Performance Analysis, Reliability*, A. Melikov Ed. Rijeka, Croatia: Intechopen, 2011. AQ6

[34] S. Sesia, I. Toufik, and M. Baker, *LTE-The UMTS Long Term Evolution: From Theory to Practice*. Hoboken, NJ, USA: Wiley, 2011. [Online]. Available: https://books.google.co.uk/books?id=beIaPXLzYKcC

[35] H. Tabassum, F. Yilmaz, Z. Dawy, and M.-S. Alouini, "A framework for uplink intercell interference modeling with channel-based scheduling," *IEEE Trans. Wireless Commun.*, vol. 12, no. 1, pp. 206–217, Jan. 2013.

[36] H. Tabassum, Z. Dawy, M. S. Alouini, and F. Yilmaz, "A generic interference model for uplink OFDMA networks with fractional frequency reuse," *IEEE Trans. Veh. Technol.*, vol. 63, no. 3, pp. 1491–1497, Mar. 2014.

Suman Kumar received the B.Tech. degree in electronics and communication engineering from the Future Institute of Engineering and Management, Kolkata, India, in 2010. He is currently pursuing the Ph.D. degree in the Department of Electrical Engineering, Indian Institute of Technology, Madras, India. He is the recipient of a Best Paper Award at ICWMC-2012 held at Venice, Italy.

His research interests are broadly in the areas of performance analysis of mobile broadband wireless networks including frequency reuse, HetNets, hypergeometric functions, and generalized fading models.

Sheetal Kalyani received the B.E. degree in electronics and communication engineering from the Sardar Patel University, Gujarat, India, in 2002 and the Ph.D. degree in electrical engineering from the Indian Institute of Technology, Madras, India, in 2008. She was a Senior Research Engineer in Centre of Excellence in Wireless Technology, Chennai, India, from 2008 to 2012. She is currently an Assistant Professor in the Department of Electrical Engineering, Indian Institute of Technology, Madras.

Her current research interests include HetNets, extreme value theory, hypergeometric functions, generalized fading models, and statistical learning algorithms for prediction.

IEEE Proof

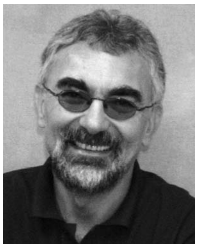

Lajos Hanzo (M'91–SM'92–F'04) received the degree in electronics in 1976 and his doctorate in 1983 from the Technical University of Budapest, Budapest, Hungary. In 2009, he was awarded an honorary doctorate by the Technical University of Budapest, and in 2015 by the University of Edinburgh. During his 38-year career in telecommunications, he has held various research and academic posts in Hungary, Germany, and the U.K. Since 1986, he has been with the School of Electronics and Computer Science, University of Southampton, U.K., where he holds the Chair in telecommunications. He has successfully supervised about 100 Ph.D. students, co-authored 20 John Wiley/IEEE Press books on mobile radio communications totalling in excess of 10 000 pages, published over 1500 research entries at IEEE Xplore, acted both as TPC and General Chair of IEEE conferences, presented keynote lectures, and been awarded a number of distinctions. Currently, he is directing a 60-strong academic research team, working on a range of research projects in the field of wireless multimedia communications sponsored by industry, the Engineering and Physical Sciences Research Council (EPSRC) U.K., the European Research Council's Advanced Fellow Grant, and the Royal Society's Wolfson Research Merit Award. He is an enthusiastic supporter of industrial and academic liaison and he offers a range of industrial courses. He is also a Governor of the IEEE Vehicular Technology Society. During 2008–2012, he was the Editor-in-Chief of the IEEE Press and a Chaired Professor also at Tsinghua University, Beijing. His research is funded by the European Research Council's Senior Research Fellow Grant. Dr. Hanzo has over 22 000 citations. For further information on research in progress and associated publications, please refer to http://www-mobile.ecs.soton.ac.uk.

K. Giridhar (M'XX) received the B.Sc. degree in applied sciences from PSG College of Technology, Coimbatore, India, the M.E. degree in electrical communications from Indian Institute of Science, Bangalore, India, and the Ph.D. degree in electrical engineering from University of California, Santa Barbara, Santa Barbara, CA, USA. AQ7

He is a Professor at the Indian Institute of Technology Madras (www.iitm.ac.in), Chennai. During 1989 and 1990, he was a Member of Research Staff at CRL, Bharat Electronics, Bangalore, and during 1993 and 1994, was a Research Affiliate in electrical engineering at Stanford University, Stanford, CA, USA. Since 1994, he has been with the Department of Electrical Engineering, Indian Institute of Technology, Madras (ITTM). He has been a Visiting Faculty at Sri Sathya Sai Institute of Higher Learning, Prasanthi Nilayam, Andhra Pradesh, and at Stanford University. His research interests are broadly in the areas of adaptive signal processing and wireless communications systems, with an emphasis on various transceiver algorithms, custom air-interface design for strategic applications, and performance analysis of mobile broadband wireless networks including HetNets.

Dr. Giridhar is a member of the Telecommunications and Computer Networks (TeNeT) Group (www.tenet.res.in) at IITM. He actively collaborates with the Center of Excellence in Wireless Technology (www.cewit.org.in) on MIMO-OFDM broadband access research, resulting in several contributions to IEEE 802.16m, and currently on proposals to LTE-A and 5G forums. He serves as a consultant to many telecom & VLSI companies in India, and was on a sabbatical in 2004–2005 with Beceem Communications.

IEEE Proof

AUTHOR QUERIES

AUTHOR PLEASE ANSWER ALL QUERIES

AQ1 = Please provide keywords.
AQ2 = Please provide department name for IIT, Madras.
AQ3 = Please provide publication update in Ref. [16].
AQ4 = Please provide publication update in Ref. [17].
AQ5 = Please provide publication update in Ref. [21].
AQ6 = Please provide page range of chapter for Ref. [33].
AQ7 = Please provide membership history for K. Giridhar.

END OF ALL QUERIES

IEEE Proof